In situ shear modulus measurements in a fractured high porosity chalk mass

Róisín Buckley[1], Ninad Shinde[2], and Luke Rieman[3]

[1]Senior Lecturer, James Watt School of Engineering, University of Glasgow, Glasgow, UK
roisin.buckley@glasgow.ac.uk (corresponding author)

[2]Post Doctoral Research Associate, James Watt School of Engineering, University of Glasgow, Glasgow, UK ninad.shinde@glasgow.ac.uk

[3]PhD candidate, James Watt School of Engineering, University of Glasgow, Glasgow, UK
luke.rieman@glasgow.ac.uk

ABSTRACT

This study explores in situ small strain shear modulus in low density structured chalk, a key input parameter in empirical and numerical models. A range of in situ testing procedures, supported by detailed core logging, have highlighted the difficulties and opportunities in characterising the in situ shear modulus of the stiff fractured chalk mass. Over 1000 seismic traces, obtained from tightly-controlled PS logging, borehole geophysical and seismic cone penetration testing were assessed for data quality. Interpretation using the automated cross-correlation technique demonstrated robustness while more time-consuming and subjective approaches were essential for lower quality data. Where comparable measurements were taken, the results tended to be relatively consistent between measurement techniques.The spacing and nature of fractures in the mass was shown to influence the results. The in situ shear modulus from seismic and pressuremeter tests tended to increase steadily from relatively low values at ground level. Sharp increases were seen at the water table, where the fractures became partly-closed and water-filled, with a weak tendency to increase with depth or burial stress thereafter. While laboratory shear modulus significantly exceeded the in situ values in the shallower layers, the results are shown to converge with depth as

the fracture frequency reduces. The new in situ shear modulus profile offers important insights and input parameters for chalk-structure interaction models. Based on the results, guidance is offered for obtaining high-quality measurements in structured chalk masses for engineering applications.

Keywords chalk, small strain, shear wave velocity **Words** 7641 **Figures:** 16 **Tables:** 5

INTRODUCTION

The small-strain shear modulus, G_0 is a key parameter in onshore and offshore site characterisation, supporting empirical design methods and the calibration of numerical models (Mayne 2020; Taborda et al. 2019). Where retrieving samples representative of in situ conditions is challenging, in situ tests are often preferred over laboratory techniques such as bender elements (BE) or the resonant column (RC) (Stokoe 2008). In the field, G_0 is calculated from shear wave velocities, V_s, measured during invasive geophysical tests. Receivers placed below ground measure the travel time, Δt, of shear waves generated on the surface (Clayton 2011). The seismic resolution depends on both the assumed ray path and the wavelength, λ (i.e. frequency and V_s). While it is typical to assume that waves travel in rays, the ray paths seen by the receivers are the result of several waves interfering inside a volume of material along the ray path. As either the wavelength or the ray path length increase, the shear waves are exposed to larger volumes of material. The resulting V_s values represent the "smearing" of the sampled material (Cox et al. 2018). The assumed ray path distance, ΔL, is used to determine the velocity and G_0 can be calculated using elastic theory:

$$G_0 = \rho V_s^2 \tag{1}$$

where ρ is the material density. To measure G_0 accurately, it is crucial to obtain precise profiles of V_s, since the former is squared in Eq. 1. Shear waves can be generated in various modes e.g. $V_{s,vh}$ refers to vertically-propagating, horizontally-polarised shear waves such as are common in down-hole (DH) seismic testing where a hammer strikes the end of a beam and the shear waves travel vertically downwards. Onshore, down-hole testing is typically conducted in water-filled cased boreholes grouted to the surrounding formation or as part of a seismic cone penetration test

(SCPT). Onshore SCPTs are often limited by the reaction force available to push the cone to depth (≈30 tonne). In the offshore environment, where installation of cased grouted boreholes is difficult, SCPTs can be installed from the seabed or, for deeper penetrations, by pushing the probe from the bottom of a drilled borehole (Lunne 2010). PS logging (PSL) in open boreholes is also commonly employed in offshore projects (Hen-Jones et al. 2024). In the field, G_0 can also be measured using pressuremeter tests (PMT) where a cylindrical device is used to apply a uniform lateral pressure to the ground via a flexible membrane, while measuring the radial applied pressure and induced deformation. The measurements are used to obtain information on stiffness and strength (Whittle et al. 2017).

While recent studies have sought to bypass the challenges in obtaining accurate V_s measurements by training machine learning models to correlate with cone penetration test data; see e.g. Entezari et al. (2022) or Stuyts et al. (2022), there remain inherent uncertainties in the underlying V_s datasets that are rarely communicated to the end-user. Stolte and Cox (2019) examined epistemic V_s uncertainty in SCPT tests in sandy/silty soils and highlighted the variable uncertainties between different methods to interpret ΔL and Δt, particularly in the near-surface and in thin layers. They recommended that the analyst clearly specify to the end-user the method of analysis and any assumptions employed. Parasie et al. (2022)'s comprehensive overview of SCPT testing in over-consolidated clays and dense sands highlighted the influence of external noise on Δt and the choice of source/receiver ray path. Near-field effects were also found to influence results in clay at shallow depths.

Detailed comparisons of V_s obtained using different invasive test types are rare. A study in soils and hard rocks by Garofalo et al. (2016) found generally good agreement between DH and crosshole (CH) borehole geophysical results. The complicated wave propagation paths in the near surface were thought to influence the significant scatter seen in DH measurements at the fractured/weathered limestone location. They also highlighted the additional uncertainties in time estimates at rock sites where travel times for wave propagation are much smaller than in soils. Stolte and Cox (2019)'s study included a review of V_s bias between SCPT and direct-push CH tests and found median percent differences of 65% in the top 3m that reduced to 10-15% with depth and could be attributed to material anisotropy. Masters et al. (2019) and Gibbs et al. (2018) highlighted the additional difficulties in acquiring and integrating offshore datasets, including poor correlation between V_s measurements obtained using different methods and the influence of noise on SCPTs obtained in drilling mode at significant depths.

Analogous studies on method dependency and uncertainty of V_s have not yet been reported for chalk, a silt-sized soft biomicrite rock widely encountered at foundation depth across Northern Europe. Matthews et al. (2000) report some of the only measurements in the literature. They found diverse trends between the results of non-invasive surface-wave and laboratory testing of intact specimens, demonstrating the extent to which the in situ shear modulus is reduced by fracturing. At depths up to 5m, they showed ratios of laboratory small-strain shear modulus, $G_{0,lab}$,to in situ small-strain shear modulus, $G_{0,insitu}$, of >1 that appeared to depend on the degree of fracturing and the intact dry density. Vinck et al. (2022) described intensive advanced laboratory testing on low-to-medium density chalk at an established research site to support the recent 'ALPACA'/'ALPACA+' axial and lateral field pile testing on piles up to 1.8m in diameter; Jardine et al. (2023). While the laboratory strength and stiffness trends were highly consistent, the SCPT G_{vh} results exhibited large scatter, particularly above the water table, with standard deviations of up to 2 times the mean value. Limited G_{hh} and G_{hv} results from historical CH testing appeared more consistent, while the G_{vh} results from PS logging (PSL) fell well below the lowest SCPT results. BE tests on intact samples of 100mm in diameter and 200mm length showed $G_{0,lab}/G_{0,insitu}$ again much >1, in tests where discontinuities were purposefully avoided. A small number of shallow pushed-in pressuremeter tests, involving pushing a Reaming Pressuremeter (RPM) into a hole pre-formed with a dummy cone, yielded lower small-strain G_{hh} values than expected, likely a consequence of de-structuration of the chalk during insertion. Overall, the available in situ shear modulus measurements appeared both depth and method dependent and the reasons for large scatter in specific in situ tests was not well understood. This posed difficulties for the calibration of constitutive models and back analysis of the field pile tests. In order to match the ALPACA'/'ALPACA+ laterally-loaded pile responses reported by McAdam et al. (2024), Pedone et al. (2023) were forced to use a shear modulus of 0.5MPa, or ≈1/3 of the average values from scattered in situ seismic tests, which fell below even the lowest CH measurements. A similar conclusion was reached by Wen et al. (2023) in their calibration of a new axial load transfer model at the site.

This paper describes the results of new in situ measurements at the same low-medium density chalk research site utilised by the ALPACA/ALPACA+ and previous research projects (Ciavaglia et al. 2017; Buckley et al. 2018). The study was conducted as part of a wider research programme that aims to quantify and reduce the uncertainty of small-strain shear modulus measurements in key geo-materials. The aims of the chalk study were to:

- Carry out an extensive characterisation and in situ testing programme to 44mbgl, including careful drilling and sampling;
- Conduct an extensive programme of carefully-controlled in situ testing comprising SCPT, PSL, DH and CH borehole geophysics and bored pressuremeters;
- Establish the influence of the testing technique, execution, data quality and interpretation method on the results;
- Investigate the effects of in situ overburden stress, chalk properties and degree and nature of fracturing on the results.
- Provide recommendations for practical interpretation of chalk datasets for a range of geotechnical applications.

SITE DETAILS AND PREVIOUS CHARACTERISATION

The site is located in a disused quarry in Kent, England (51°21'22"N , 001°14'10"E) where structured chalk is encountered from surface. Previous characterisation has included drilling and sampling and limited PSL, CH and DH testing and the additional rotary and block sampling, cone penetration tests (CPT), SCPTs, tensiometers and RPM tests reported by Vinck et al. (2022). While the rotary boreholes described by Vinck et al. (2022) had average total core recovery (TCR) values of 74±28%, the average solid core recovery (SCR) values of 54±31% were disappointing and presented difficulties for detailed logging. The existing drilling and sampling showed that all but ≈1.6m of the pure white Margate chalk has been removed by quarrying, with the horizontally-bedded Seaford chalk with nodular flints encountered from ≈5.2m above ordnance datum (AOD). Tensiometer tests showed that the water table lies at ≈0.9±0.25mAOD. From surface to ≈-2.7mAOD, structured, very weak to weak, low-medium density chalk was encountered with discontinuities open to <3mm and spaced at 60-600mm (CIRIA Grade B3/B2); Lord et al. (2002). The grade improved to A2 thereafter, with fractures closed and spaced at 200-600mm. The maximum depth of the boreholes was ≈-9.5mAOD.

METHODOLOGY AND TESTING PROGRAMME

Drilling, sampling and in situ testing

This study targeted an area south-east of the pile tests conducted for ALPACA+. Fig. 1 demonstrates that the present study area lies outside of the zone of influence of the pile installations. Four rotary-cored boreholes were installed to between 25 and 44m below current ground level (≈6.7mAOD). Inspection pits were first hand dug to 1.2mbgl. The rig was carefully leveled to ensure verticality; post-construction surveys showed that final deviations of the tip from the vertical were 0.1-0.5°. The TCR and SCR were on average 90±18% and 73±28% respectively. Sub-samples were wrapped in layers of cling film and wax to preserve the natural water content. Following drilling, 90mm closed-end PVC casing was grouted in place using a tremie pipe, with a final density reflecting that of the chalk (ASTM: D4428, 2016). The grout was repeatedly topped up to ground surface over several days, as it migrated into the fractured mass and finally settled at ≈2mAOD. Cement bond log (CBL) testing (Winn et al. 1962) showed generally good coupling between the PVC, grout and chalk (see Fig. 2(a)). A probe, consisting of a detachable 137Cs gamma source and two scintillation detectors, was used to measure the formation density in BH4.

The CPTs and SCPTs (see Table 1) were installed using a truck-mounted rig at a standard penetration rate of 20mm/s. The SCPT module incorporated two uni-axial horizontal geophones spaced at 0.5m. Shear waves were generated on the ground surface by striking a hammer on a shear beam weighted by the CPT truck (Fig.3 (a)). The distance from the shear beam to the probe axis,

d_s, was measured precisely using a Leica TS06 total station, while checks on the penetration were made using an independent reference point above ground level. The seismic module was advanced in increments of 0.25-0.5m until refusal (see Table 2). A vibration monitor triggered the data acquisition system to begin recording. The SCPTs reached early refusal in all cases. Deeper tests were attempted in SCPT4, by pushing a "dummy" cone to depth and placing the seismic module in the pre-made hole.

Downhole and crosshole borehole geophysics

DH tests were conducted in all four boreholes. Shear waves were generated at the ground surface using a sledgehammer and a shear beam connected to a trigger (Fig. 3(b)). A pair of vertically-installed receivers, spaced at 2m, were clamped to the borehole wall using an air-inflated bladder. The receivers consisted of multi-axial BGK5 (Geotomographie) sensors comprising one vertical and 4 horizontal (H1, H2, H3, H4 in clockwise order) sensors, separated by 45°. A vehicle weighed down the shear beam to ensure good ground coupling. A reference geophone placed on the surface served as a check on trigger consistency.

A fundamental assumption in DH testing is that the profile being characterised has transverse isotropy i.e. that the velocities do not vary with azimuth (ASTM:D7400 2019). Shear Beam 1 (SB1) was placed with its long-axis perpendicular to H1, while Shear Beam 2 (SB2) was placed with its long-axis perpendicular to H3. The tests were carried out at 1m increments (Table 2) to the final depth. The entire process was repeated with both shear beams (SB1 and SB2) and both left (L) and right (R) polarisations. The shear beam was placed a distance, d_s, of 2.15m from the borehole axis and located precisely using a Leica GPS. Additional tests in BH4 investigated the influence of source offset on the results.

Cross-hole tests involved generating shear waves at 1m increments within BH4 which were measured by receivers placed at the same elevation in BHs 1-3 (Fig. 3(d)). The deviation survey (which showed that final deviations of the tip from the vertical were 0.1-0.5°) was key to precise calculation of the travel distances. Horizontally-polarised shear waves were generated using an impulse generator within a BIS-SH-DS source (Geotomographie) clamped to the borehole wall.

Energy released by the impulse generator displaced through a system of coupled coils that generated a mechanical impact to the borehole wall. Waves of opposite polarity were generated by rotating the source 180^{o} with the two directions denoted ’Towards’ and ’Away’. While vertically-polarised waves were also generated using a shear-wave hammer locked in place on the borehole wall, the signals were of poor quality (likely due to poor coupling with the borehole wall) and the results are not included. The same BGK5 system was used as a receiver in BH3. BH1 and BH2 included BGK7 (Geotomographie) multi-axial sensors comprising one vertical and six horizontal components.

PS logging

PS logging, carried out in each of the four boreholes, employed a single probe consisting of a reversible-polarity horizontal solenoid and strike cylinder arrangement aligned to two bi-axial receivers (Hen-Jones et al. 2024) and separated by filter tubes (Fig. 3(c)). The source motion creates an impulsive pressure wave in the borehole fluid which is converted, at the borehole wall, to compression and shear waves propagating in the surrounding material. These waves in turn cause pressure waves to be generated in the fluid surrounding the receivers spaced 1m apart.

The travel time difference between the two receivers is used to determine the average velocity of a 1m high column of material surrounding the borehole. The amplitude of the shear wave signals is maximised by orienting the horizontal receivers parallel to the axis of the source. Reverse polarity shear wave signals were recorded at each 1m interval. The probe was first lowered to a given depth to make stationary measurements for quality assessment and adjustments of the acquisition parameters and then lowered to the borehole base to begin testing. Tests were repeated as the probe was removed from the borehole. While PS logging is typically carried out in uncased boreholes, the tests were conducted in the PVC-cased boreholes here for logistical reasons. An additional test in BH4, prior to casing installation, served as a check on its influence.

Pressuremeter testing

Self-boring pressuremeters (SBP) were carried out in BH2 and BH4. SBPs are recommended in chalk due to the de-structuration that can be caused by pushed-in methods (Whittle et al. 2017). The SBP consists of six equally-spaced displacement transducers (expansion limit of 15%), an internal pressure transducer (capacity 10MPa) and two opposite facing pore-water pressure (PWP) transducers. The probe was set up for testing in aggressive material with the coring arrangement making a hole 1mm greater than the diameter of the expanding section. This allowed the probe to bore into stiff materials by applying a small amount of stress relief, within the recoverable range of the material (Cambridge-insitu 2023). The SBPs were installed using reaction provided by the rotary core rig resulting in only minor alterations to the in situ stress conditions. Flints can damage the SBP membrane; where they could not be avoided, RPM and High Pressure Dilatometer (HPD) tests were carried out in pre-bored pockets made using a T2-101/HWF core-barrell. The tests were conducted sufficiently slowly to allow any excess PWP generated to drain immediately. Table 3 outlines the pressuremeter testing programme. The test depth quoted is the centre of the measurement section. The length of the membrane influences the zone of chalk affected by the pressuremeter expansion. For RPMs, SBPs and HPDs these zones are ±0.13, ±0.23 and ±0.30m of the quoted test centres respectively.

Laboratory testing

Index and unconfined compressive strength (UCS) tests were used to augment the existing profiles reported by Vinck et al. (2022) and check for changes in stratigraphy in the deeper chalk layers. Resonant column tests were carried out using the Hardin Oscillator device (GDS instruments) at the University of Glasgow. The high stiffness of the chalk samples induces significant compliance in the apparatus, therefore the development of a novel calibration approach using dummy samples of representative stiffness was necessary (Rieman et al. 2024). The specimens had height-to-diameter ratios of 2-2.5 and were prepared in a similar manner to that described by Vinck (2021). To ensure good torsional coupling, grooves were cut into the sample ends and high-grade (dental) gypsum plaster was used to bond the sample to textured disks on the top cap and pedestal. Filter paper drainage strips allowed pore fluid to bypass the low-permeability plaster. Samples were saturated and then consolidated isotropically to effective stresses representative of in situ conditions. After consolidation, each sample was allowed to creep for at least 24hrs, or until volumetric strain rates fell below 0.01%/day, before resonance testing. Selected results from the intensive programme of

RC testing on intact samples are included here.

INTERPRETATION OF SEISMIC DATA

The 1157 traces analysed from DH, CH, PSL and SCPT testing required treatment prior to interpretation. In all cases, multiple repeat tests or "shots" were taken and the data stacked to increase the signal-to-noise ratio. Typical frequency spectra for each test type in this formation are shown on Fig. 4. The PSL signal's comparatively high dominant frequency of around 1.8kHz is designed to propagate with a short wavelength, only sampling a relatively short distance ($\lambda \approx 0.5$m for V_s = 900m/s) from the source. The DH, CH, and SCPT testing signals all have peaks <300Hz. These lower frequency waves propagate with a longer wavelength stressing materials and sampling properties to greater depths.

Based on the spectra shown in Fig. 4, a low-pass filter (Baziw 1993) was applied with a cut-off frequency, f_c, selected to remove unwanted noise and additional artifacts. The filter employed, a zero phase-shift Butterworth filter, ensured phase shifts were not introduced. In some cases, signal windowing (Prabhu 2014) was used to minimise distortion due to different propagating modes. A Hamming window function was used to create smooth, tapered windows of a dominant single cycle; Liao and Mayne (2006). This was only necessary in the CH and SCPT testing and represented in total $\approx$6% of cases (see Table 4). All of the acquired data complies with the Nyquist theorem i.e that a band limited signal is completely described if it is sampled with at least the double of the maximum signal frequency. It is noted however, that the SCPT sampling frequency of 5kHz resulted in a sampling interval of 0.2ms and therefore calculated Δt values in multiples of 0.2ms. When combined with the small travel distance between the SCPT receivers of 0.5m, and the relatively high V_s values, this led to insufficient accuracy in shear wave velocity (Rice 1984). The SCPT samples were therefore up-sampled to a 100 times higher rate using the MATLAB algorithm *resample* in a similar approach to that employed by Karl et al. (2006).

For the dual-receiver arrangements employed, V_s is calculated by dividing the difference in wave travel path length between the two receivers, ΔL by Δt;

$$V_s = \frac{L_2 - L_1}{t_2 - t_1} = \frac{\Delta L}{\Delta t} \tag{2}$$

The first step in the analysis involves assessing the true-interval travel times, Δt between receivers at vertical distances, d_1 (R1) and d_2 (R2) from ground level, where $d_2 > d_1$; Fig. 3. Stolte and Cox (2019) provide a comprehensive review of methods to estimate Δt. The cross-correlation (CC) technique (Campanella and Stewart 1991; Baziw 1993) is typically considered the most accurate since it uses information from the whole signal, can be easily automated and is relatively free of human bias. The CC function of a signal Y_k sampled at d_2 and sample time k and a signal X_k sampled at d_1 and sample time k is:

$$\varphi_{xy}(t) = \sum_k X_k Y_{k+t} \tag{3}$$

The value of the time-lag at the peak of the function is equal to Δt. Other approaches utilised (see Fig. 5) included methods to compare relative travel times between (i) dominant peaks (P-P) on both signals and (ii) characteristic cross-over points on the signal of signals of reverse polarity (RP) (e.g. before dominant peak). All three methods to calculate Δt (CC, P-P and RP) were applied to each of the measurement depths/locations and the relative performance of each method was assessed.

The second step in the analysis involves making an assumption on the ray-path distance between source and receiver. DH, PSL and SCPT employed Eq. 2 with distances L_1 and L_2 as defined on Fig. 3. The CH testing also used Eq. 2 but with horizontal distances. A straight-ray assumption between source and receiver was assumed since (i) the data was relatively scattered in the top metres preventing detailed ray-tracing and (ii) the source offsets were small indicating primarily vertical travel paths. In more complex profiles, or for large source offsets, leading to large angles of incidence between the source and horizontal soil layers, refracted wave paths often need to be considered under the assumption of a laterally homogeneous medium.

Assesment of data quality

An assessment of data quality for seismic signals can help analysts to make relative judgements on individual measurements. The cross-correlation coefficient (CCC), obtained by normalising the CC of two signals at successive depths by their standard deviations, can give an indication (0 indicating no correlation, 1 indicating perfect correlation). However CCCs alone are known to be unreliable indicator since correlated measurement noise can result in misleading high coefficients. Baziw and Verbeek (2017) proposed a data-quality classification that augments the CCCs with additional quality indicators (Fig. 6). For two signals at depths d_1 and d_2 the Seismic Trace Characterisation (STC) is:

$$STC = 0.4CCC + 0.18(Lin_1 + Lin_2) + 0.12(SSP_1 + SSP_2) \tag{4}$$

The linearity (Lin_1/Lin_2) estimates quantify the correlation between the responses measured on orthogonal horizontal axes (e.g. H1 and H3) at successive depths. Linearity values close to one indicate low measurement noise, clean source waves and little unwanted reflections. Low values suggest reflections, ambient noise or poor source-wave quality. The signal shape parameter (SSP) is a measure of the deviation of the frequency spectrum from the probability density function (pdf) of a Gaussian distribution. The value of SSP ranges from 1 (high-quality) to 0 (poor-quality); see Fig. 6. The SCPT employed uniaxial receivers for which a modified form of Eq. 4 was employed; (BCE 2020):

$$STC_{scpt} = 0.6CCC + 0.2(SSP_1 + SSP_2) \tag{5}$$

For the comparatively high-frequency PSL data, linearities were used in place of SSP in Eq. 5. Eq. 4 and 5 were calibrated by Baziw and Verbeek (2017) from 4000 traces at 40 sites and given a classification from A(0.8-1) to F(<0.65). They note that STC values <0.65 should be evaluated carefully and not subjected to batch or automated processing. While the classification may not be fully calibrated for chalk, the STC proved invaluable in assessing the relative quality of the large number of signals obtained. It was particularly useful in guiding the choice of method to calculate

Δt. Since STCs were developed and calibrated using a database of downhole tests, it was not appropriate to apply the same framework to the CH dataset.

RESULTS AND ANALYSIS

Chalk stratigraphy and classification

Core Logging

Fragmented core and drilling-induced fractures present difficulties in the representative logging of chalk (Mortimore 2022). Core-logging of the high TCR and SCR boreholes provided important insights for the interpretation of the in situ tests. Fig. 7 charts a cross-section across the study area showing the main features observed, along with the fracture index (FI) - the average number of fractures per metre. The base of the Margate chalk Member, evidenced by the observation of Barrois' sponge bed at ≈5mAOD, coincided with the bottom of the inspection pits therefore only the Seaford chalk formation was encountered in sampling. Well-structured, clean, very weak-to-weak white chalk was encountered throughout the boreholes. From surface to ≈-4mAOD, the fractures were slightly open and spaced at 150-200 mm (CIRIA grade B3/B2), typically sub-horizontal and sub-vertical and moderately speckled/stained. The chalk includes few small-medium (<50-100mm) nodular flints. More frequent and larger (100-150mm) flints were encountered in BH2 and particularly in BH4 between 2 and -2mAOD. From ≈-4mAOD the chalk grade improved to A3/A2 with fractures mostly closed and spaced 170-400mm. A zone of significant core loss between -5.9 and 6.6mAOD could be attributed to local dissolution or a weaker bed (Lawrence 2024). The flint bands became more regular with depth and a zone of fragmented and larger flints >100mm at ≈-7mAOD signalled the presence of Whitaker's Three Inch flint band (Aldiss et al. 2004). Orange iron-stained sponge beds were occasionally encountered, evidence of local colonisation on the original chalk floor (Mortimore 2014). From ≈-21.5mAOD the fracture spacing reduced to 300-1000mm (Grade A2/A1) up to the end of borehole at ≈-37mAOD.

Index properties and in situ testing

Selected index properties are plotted in Fig. 2 along with the data from Vinck et al. (2022). The results indicate little change in properties over the sampled profile. The sampled chalk's intact dry density, ρ_d of 1.43-1.53 Mg/m^3 showed little variation in with depth. The bulk densities, ρ_b, also varied very little with depth ranging from 1.91-1.98 Mg/m^3 with an average of 1.95Mg/m^3. The laboratory values lay just below the average ρ_b of 2.05±0.07Mg/m^3measured by the gamma probe. The degree of saturation is close to 100% up to ground surface. The water contents, of 28-32%, lie close to or just below the liquid limit, leading to the chalk's susceptibility to puttify under high compressive loads; Buckley et al. (2018). The plasticity indices of the new samples of ≈10% was higher than the 7.8% reported by Vinck et al. (2022) and the 6.6% reported by Bialowas et al. (2016) for the same material, possibly reflecting the natural subjectivity of the test/preparation procedure. The UCS strengths, q_u, also remain consistent with depth with an average of 2.7±0.3MPa from 10 samples.

Fig. 8 plots the CPT traces completed for this study (CPT1-5) along with the pre-pile installation CPTs conducted at the ALPACA+ site (+NA01-03 see Fig. 1), closest to the study area. The corrected cone resistances, q_t, from the new CPTs follow the same trends as previously, lying between 5 and 35MPa with spikes seen in thin, discontinuous, flint bands. The flint bands materialised at shallower depths at the current study area, as also seen in the boreholes, leading to early refusal in all but CPT3. When taking the decision to stop a test, the operator made judgements based on the total thrust being applied to the cone, the tip resistance, the cone capacity, and the conditions through which the cone had already passed. Deeper penetrations may have been possible with different cone configurations and additional reaction force. The sleeve friction, f_s, and excess PWP measured at u_2 also follow previous trends; f_s ranges from 50-1000kPa and u_2 up to 7MPa is measured as the chalk de-structures beneath the cone tips. Still higher pore pressures at the u_1 position, of up to 10MPa, were reported by Buckley et al. (2021). Local layers of low resistance were observed at depth at both areas (see e.g. CPT3 between -3 and -5mAOD), with q_t reducing to 1MPa or lower and f_s to <50kPa, accompanied by sharp drops in u_2. The low resistance layer in CPT3 lies just above a zone of core loss seen in the nearby BH2, with CBL testing (see Fig. 2.) also indicating the presence of a possible void around -6mAOD.

Profiles of shear wave velocity

Downhole testing

The STCs show markedly different trends above and below the water table and facilitated screening for data quality. Above the water table at ≈0.9mAOD, the STCs are typically 0.2-0.5, possibly reflecting the more complicated wave paths followed in the slightly open air-filled fractures and/or poorer quality grouting (CBL testing was not possible in this region). Below the water table, the STCs of 0.8-1.0, indicate excellent data quality. All three methods to calculate Δt (CC, P-P and RP) were applied to each of the measurement depths/locations. The following trends were observed (see Fig. 9 (a) and Table 4):

- CC gave clear unambiguous results for ≈92% of the data. In the remainder of cases, CC was influenced by near surface reflections and poor correlations between the two signals, leading to erroneously high or low Δt values for these materials, particularly where the dataset was of lower relative quality above the water table.
- Below the water table, although more subjective and manual, the P-P method gave broadly consistent, but more scattered, results to the CC with ≈80% of the data plotting within ±20% of the CC result.
- The RP method was only reliable where a clear cross-over point could be chosen objectively with final results showing a scattered trend with only ≈50% of resulting V_s lying close to the PP or CC value.

The following interpretation primarily utilises the CC approach to calculate Δt and therefore V_s. Where the CC function led to errors, in 8% of cases, the interpretation was advanced by first trialling the P-P method. If clear peaks could not be identified, the RP method was then utilised. The latter was used for 4% of the signals. A portion of the records above the water table were discarded e.g. in cases where where reflections led to intractable arrival times or where the shear wave arrived at R2 before R1.

Profiles of $V_{s,vh}$ interpreted from DH testing are presented in Fig. 10. The results of polarised traces from SB1 recorded by the most relevant sensors are primarily presented. The symbols on the plot are shaded according to STC while the grey-shaded regions represent the the mean±one standard deviation, σ. As noted above, the trends in STC reflect the relative scatter apparent in the results. Below the water table, the $V_{s,vh}$ values are remarkably consistent with average values typically of 880m/s and σ values of <5% of the mean. Above the water table, where the fractures are partly-open, air-filled and typically spaced at ≈150mm, the average $V_{s,vh}$ of 583±86 m/s is significantly lower. Decreasing fracture spacing and aperture was shown by Matthews et al. (2000) to decrease the in situ shear wave velocity of chalk. The results in this region are also more scattered, which may reflect natural variation in the chalk stiffness. McAdam et al. (2024) noted variation in load-displacement behaviour of simultaneously laterally-loaded piles that they attributed to variation in the chalk mass stiffness. The relative scatter in this region may also be partly attributed to the deviation of the wave travel path from the straight ray assumption. It is noted however, that the values are consistent between different sensors and source offsets (see Fig. 11) giving confidence in the interpreted values.

The mean $V_{s,vh}$ at -35.8mAOD in BH4 was 934m/s at an in situ vertical stress of ≈480kPa representing a remarkably weak trend for $V_{s,vh}$ to increase with burial depth. Fig. 7 shows that the fracture spacing increases from ≈150mm at the water table to ≈500mm at the base of BH4, with the fractures primarily closed or slightly open from -4mAOD. The marginal increases in $V_{s,vh}$ with depth may reflect both the change in fracture pattern and increasing in situ stress level. Liu et al. (2022) characterised the chalk's shear modulus over a wide range of stress levels in high pressure laboratory tests, and found that G_0 is controlled by the chalk's cemented particle structure and the closure of fissures at high stress levels. The 2m spacing of the DH receivers resulted in $V_{s,vh}$ values that were relatively unaffected by soft zones or significant flint bands, with the exception of the zone of larger and more frequent flints seen in BH4, which is reflected by a spike in $V_{s,vh}$ at around -2mAOD. While the STCs resulting from tests with SB2 were marginally lower than the SB1 results, possibly due to a less robust connection between the beam and metal plate, the $V_{s,vh}$ results were in good agreement with average differences typically of 5-10%.

Crosshole testing

While CH testing is often considered more reliable than downhole testing, since the waves are generated and measured at the same depths, CH tests can be influenced by factors such as poor signal source generation, poor PVC-grout-chalk coupling, and refracted waves from stiffness contrasts. STCs were not appropriate for the CH data, therefore it is difficult to make relatively judgements on data quality. However, application of the three interpretation methods to calculate Δt led to significant scatter in V_s between the three methods (see Fig. 9 (b)). The following interpretation utilised the RP approach in ≈60% of cases (see Table 4), since it allowed the most consistent picking. Cross-correlation was utilised where clear cross-over points in RP could not be identified (14% of cases) with CC with windowing proving successful for 24% of signals where poor grouting was thought to influence data quality. This deliberate data reduction technique was significantly more time consuming than the DH testing, reflecting a likely poorer quality data set.

Fig. 12 plots the interpreted $V_{s,hh}$ values from crosshole testing. The BH2/BH1 and BH4/BH3 results showed that the $V_{s,hh}$ lies close to the mean DH $V_{s,vh}$ trend with values of 867±63 m/s below the water table and little lateral variation in $V_{s,hh}$. Above the water table, the results indicate consistently lower average values of 631±186m/s, also plotting within the DH $V_{s,vh}$ range. The profiles shown in Fig. 12 suggest that the CH configuration was more sensitive to local variations in the chalk properties than the DH testing, e.g. the higher velocity layers associated with the significant flint bands seen in BH4 between 2 and -2mAOD. The results obtained between BH3 and BH2 (see Fig. 12 (b)) were lower and more scattered at the possible void location (identified in CPT3 between -3 and -5mAOD and in BH2 at -6mAOD) and in regions where PMT tests had disturbed the material and the grout showed poorer quality (see Fig. 2).

Seismic cone penetration tests

Seismic cone penetration tests are not commonly conducted in soft rocks since high forces are generated from tip resistance and friction on the cone and rods that can overload the capacity of the equipment. While SCPTs can be carried out in sensitive soft rocks such as chalk, their penetration can still be limited by equipment geometry and available reaction force. In this study, the SCPTs' early refusal resulted in a maximum penetration of -2.25mAOD. The STCs were generally high, with values >0.9 in most cases. Traces collected after pushing to depth with a dummy cone were disregarded as inclinations and twist led to erroneous results. Since reverse polarity data was not acquired, it was only possible to apply the PP and CC methods to the SCPT data, The P-P and CC results were relatively consistent with each other, particularly where windowed signals were used in the CC (see Fig. 9 (b)). The following interpretation primarily used CC with P-P utilised in cases where poor correlation was seen between the signals; see Table 4.

Fig. 13 (a) plots the mean $V_{s,vh}$ results from SCPT1-6 along with error bars that denote the standard deviation across 10 repeat shots. The results show the largest scatter close to the surface where $V_{s,vh}$ ranges from ≈200-600m/s reducing with depth as the results fall towards the DH and CH trends. Also shown on Fig. 13(a) is the range of maximum and minimum $V_{s,vh}$ from the previous SCPT tests at the site. The scatter, which may be attributed to both natural variation and difficulties in test execution or data acquisition/reduction, is shown to be significantly reduced in the tightly-controlled tests conducted for this study, with the new test results falling at the lower end of the previous range.

The limited overlap of SCPT and DH $V_{s,vh}$ measurements reduces the detailed comparisons that can be made between the two test types. Above the water table, the mean SCPT trend from across the site (see Fig. 13 (b)) plots ≈50% above the DH site mean. This may reflect the additional travel time uncertainties associated with the lower 0.5m spacing of the SCPT sensors and the relatively high chalk shear wave velocities; see Garofalo et al. (2016) combined with the complicated wave paths followed in the fractured material. Lateral variation in chalk properties may also play a limited role. The divergence between the two sets of measurements reduces with depth or improving chalk grade;below ≈2mAOD there is good agreement between the measurements.

PS logging

The geometry of the PSL probe led to the first measurements occurring at ≈0.5mAOD, ≈1.5m below the top of the grout. The STCs were typically close to 0.8 indicating excellent quality with values of around 0.5 highlighting traces requiring additional analysis. Fig. 9 (c) gives an example of the PSL interpretation of Δt using all three methods. Again the automated CC or CC with window approach gave consistent results in 86% of cases with the remaining giving erroneously high and low data points associated with poorly correlated signals. These remaining CC V_s results showed a scattered trend when compared with the RP and PP approaches, which gave similar results with ≈85% of V_s values lying within 20% of each other. The following interpretation again primarily used the CC approach with the P-P and RP methods used in cases where the CC did not find a suitable correlation.

Fig. 14 plots the $V_{s,vh}$ outcomes from tests in each of the four (cased) boreholes. The results from L and R polarised waves show remarkable consistency with $V_{s,vh}$ values of 892±88m/s. The PS logging results followed the trends seen in the DH with little variation seen with depth. The 1m receiver spacing, combined with the test interval of 0.5m led to a higher vertical resolution in the shear modulus. Also shown on Fig. 14 are the results from the SCPTs conducted close to and prior to the installation of BH2 and BH3. Where direct comparisons can be made below the water table, the SCPT trend lies close to the PSL results, both lying slightly above the mean site DH trend. Comparison of the logging results in the uncased and cased BH4 showed that the average difference between tests at identical depths was ≈4%.

Laboratory and in situ shear modulus trends

Pressuremeter testing

Fig. 15(a) plots pressure at the cavity wall versus cavity strain for all of the successful PMTs. Comparison of the SBP and pre-bored (HPD/RPM) curves indicates very similar behaviour; pre-boring does not completely destroy the chalk structure, as was seen in earlier pushed-in tests. The primary aim of the PMTs was to obtain estimates of the in situ shear modulus. Despite their high resolution, it is generally not possible to measure G_{hh} directly due to limitations of the control system. Obtaining an estimate of G_{hh} requires assuming that the material (i) is homogeneous and isotropic (ii) behaves as a continuum and (iii) is fully saturated. End effects are assumed to be negligible. The initial loading is heavily influenced by disturbance and the subsequent unloading of the cavity wall and as a result, unload-reload loops are used to characterise the maximum G_{hh}.

Bolton and Whittle (1999) showed that the non-linear stiffness response on the unload-reload path is well represented by a power law, where the exponent, β, defines the non-linearity of the response and α is the shear stress constant. This approach allows the shear modulus degradation, from the maximum G_{hh} value at the elastic threshold to the yield strain at which full plasticity is initiated, to be modelled. The expression for the secant shear modulus, $G_{s,hh}$, as a function of shear strain, γ, is therefore:

$$G_{s,hh} = \alpha\gamma^{\beta-1} \tag{6}$$

Eq. 6 can be used to calculate the variation in secant modulus over a range of strain levels. Multiple loops within each test in the chalk indicated that the stress applied at the cavity wall eventually initiated collapse of the chalk skeleton. An increase in stiffness with successive unload/reload cycles was seen, due to increases in the mean effective stresses during expansion. The power law trend (Eq. 6) that best represented the shear modulus at the in situ stress state was identified. The parameters are shown in Table 5 while Fig. 15 (b) plots the trend for each of the tests shown in part (a).

It can also be inferred from Cao et al. (2002) that there is a relationship between G_y and G_{hh}, such that $G_{hh} = G_y Exp(1/\beta)$, where G_y is the shear modulus at first yield of the material. The tests indicated that yield occurred in the chalk at a shear strain of ≈0.2%. The resulting maximum G_{hh} values, which are typically conservative (Byrne and Whittle 2023), fall in a relatively wide range of 1.3±0.6GPa in four of the five cases, equivalent to V_s of ≈820±550m/s. One test, BH2 Test 6, gave a much lower G_{hh} value of 378MPa, possibly reflecting disturbance or a lower resistance zone such as was seen at shallower depths. Fig. 15 (b) also plots the previous pushed-in tests conducted at similar stress levels, demonstrating the influence of the insertion process on the results.

Combined trends in shear modulus with depth

Fig. 16 plots the average trends in G_{vh} and G_{hh} (calculated using the average value of ρ_b of $1.95 Mg/m^3$ discussed previously) acquired from across the testing area, obtained by interpolating between data points for individual profiles, along with selected laboratory tests from BE and RC testing on site samples and the FI from detailed logging. There is a clear trend for G_{vh} to increase from low values of ≈300MPa at the surface to an average of ≈800MPa at 2mAOD. The results indicate average G_{vh} values of 300 to 600MPa over the extent of the 3.05m long ALPACA laterally-loaded piles (McAdam et al. 2024), close to the value of 500MPa required to match the results of field tests by Pedone et al. (2023). At the water table, G_{vh} increases sharply to ≈1.5±0.2MPa and remains relatively stable with depth or increasing stress level up to the maximum depth of ≈43m. The crosshole G_{hh} results follow a similar trend, indicating values of 400 to 700MPa above the water table that then stabilise at ≈1.5±0.2MPa. Comparison between average G_{vh} and G_{hh} in the shallow and deep chalk layers indicates anisotropy ratios G_{hh}/G_{vh} of ≈1±0.15 over the entire profile. While the PMT trends show greater scatter in G_{hh} their typical range of G_{hh}=1.3±0.6GPa is consistent with the seismic results.

The available RC and BE results shown on Fig. 16 highlight the marked differences between the shear modulus obtained in the laboratory and the shear modulus applying in situ. The laboratory results indicate average shear modulus values of 2.2±0.2GPa over the profile that showed modest variations with depth and stress level. The $G_{0,lab}/G_{0,insitu}$ ratios fell from almost 8 at ground surface to stable values of 1.44±0.17 from the water table to the final investigation depth. As the chalk grade improves and the FI reduces with depth, the ratios move closer to 1. Full agreement between the laboratory and in situ test results is unlikely since laboratory tests must employ purposely uniform samples free of discontinuities, which cannot adequately reflect the in situ chalk mass properties.

SUMMARY AND CONCLUSIONS

This study has investigated the influence of both test-specific and material-specific factors on profiles of in situ small strain shear modulus in chalk. The following main conclusions are drawn from the study:

- Detailed logging of high-quality chalk cores identified key features, including how flint frequency varies both laterally and with depth and identified the presence of low resistance zones or voids. Logging and index testing highlighted the consistency of the chalk unit to depths of 44mbgl.

- A suite of tightly-controlled and carefully-conducted in situ testing has been executed including downhole and crosshole geophysics, PS logging and seismic cone penetration tests. The seismic trace characteristic suggested by Baziw and Verbeek (2017) facilitated screening of the geophysical data, a targeted interpretation approach and removal of erroneous traces.
- In the majority of cases, interpretation of elapsed travel times using the automated cross-correlation technique yielded consistent results with high CCC and limited scatter. More subjective and time-consuming approaches, that compare characteristic points on the signals (peaks and cross-over points in reverse polarity signals) were shown to give similar results in cases were the data quality was acceptable.
- Downhole borehole geophysics yielded remarkably consistent results between multiple receivers and showed a weak tendency for $V_{s,vh}$ to increase with depth, up to ≈43m below ground level or an insitu stress of ≈480kPa. The $V_{s,vh}$ results for these tests, where the receivers were placed 2m apart, were relatively unaffected by higher strength flint bands and soft zones within the chalk.
- The cross-hole tests, which were conducted every 1m and with source and receiver at the same level, resolved local variations in G_{hh} to a greater extent than the DH tests and overall indicated anisotropy ratios close to 1.0. Self-bored/pre-bored pressuremeter tests are shown to give highly representative results in chalk where flint bands can be avoided. The PMTs confirmed the G_{hh} trend seen in the crosshole tests.
- PS logging also gave highly consistent trends in $V_{s,vh}$ up to 42m depth that mirrored the DH values, at higher vertical resolution than the DH tests.
- Execution and intepretation of SCPTs in chalk can be difficult; high installation forces can lead to early refusal and the low receiver spacing combined with high wave velocities can introduce additional uncertainties in travel time estimates. Where SCPT $V_{s,vh}$ overlapped with other methods, the SCPT tended to fall closest to the PSL trend.

- The overall trend in in situ shear modulus at the site, is for the values of G_{vh} and G_{hh} to increase from relatively low values at ground level. Sharp increases are seen at the water table where the fractures become partially closed and water-filled. As the stress level or depth increases, and the fractures become less frequent, the shear wave velocity increases only slightly up to >40m below ground level.
- The results highlight the trend for laboratory shear moduli to lie well above the field values in some cases due to the influence of fracturing and fissuring in the chalk mass. The current study, which involves investigation to significant depths relative to foundation levels, demonstrates for the first time that as the fractures close, and become more widely spaced, this ratio approaches 1.
- The outcomes provide important insights into, and guidance on, taking high quality measurements in structured chalk masses that will be useful for several engineering applications. The new in situ shear modulus profile will also aid the interpretation of field experiments conducted at the site.

RECOMMENDATIONS FOR PRACTITIONERS

This study has highlighted the importance of a targeted approach to test execution and data acquisition in (relatively) high velocity materials such as chalk. Each of the in situ testing methods presented in this paper has relative merits and where comparable measurements could be made there appears to be small differences between the values of in situ shear shear modulus obtained. High quality samples are required for representative core logging and the choice of in situ testing technique should consider the nature and frequency of fracturing as well as the particular application. For applications in similar materials that require G_{hh}, such as laterally loaded piles, downhole testing may be used in place of crosshole testing due to the limited in situ anisotropy. Where characterisation of thin layer features is required, e.g. for tunnelling applications, the identification of flint bands and dissolution features may be more robust where depth increments are chosen following detailed core logging. In the offshore environment, where downhole and crosshole borehole geophysics are difficult to execute, PSL is likely to be the most suitable current method to obtain representative profiles in chalk. As noted, the chalk's mass stiffness is controlled by the network of fractures present in the chalk mass, leading to poor correlation with laboratory element tests and highlighting the requirement to take in situ measurements for use in geotechnical analyses. Importantly, where only laboratory shear moduli are available for use in design, designers should make careful judgements to reduce the values to account for the in situ chalk's micro to macro fissuring pattern.

ACKNOWLEDGMENTS

The SOURCE project is funded by the Engineering and Physical Science Research Council (EPSRC) grant EP/W020807/1. Rieman is supported by the University of Glasgow through the EPSRC Doctoral Training Partnership. The support of the project's industrial partners in carrying out the fieldwork and supporting the interpretation is gratefully acknowledged: Cambridge In situ Ltd (Robert Whittle and Yasmin Byrne), In situ site investigation (Darren Ward and Luisa Dhimitri), RobertsonGEO (Graham Comber and Rosalind Hen-Jones) and RSK (Tim Grossey, Chris Gorman and Jessica Slamaker). The diligence and patience shown by A2 Site Investigation, who carried out the drilling and sampling to a high standard, is appreciated. The contribution of Michal Ozarek's MEng dissertation to the laboratory work is also gratefully acknowledged.

REFERENCES

Aldiss, D., Bloomfield, J., Buckley, D., Doran, S., Evans, D., Hopson, P., Royse, K., and Woods, M. (2004). "A geological model of the chalk of east kent." *Report*, British Geological Survey.

ASTM:D7400 (2019). "Astm d7400—19: Standard test methods for downhole seismic testing.

Baziw, E. and Verbeek, G. (2017). "Quality assessment of seismic data sets and the impact on interval velocity estimates in dst." *DFI 42nd Annual Conference on Deep Foundations*.

Baziw, E. J. (1993). "Digital filtering techniques for interpreting seismic cone data." *Journal of geotechnical engineering*, 119(6), 998–1018.

BCE (2020). "Bce sc1-rav™ 2020 seismic data analysis software manual v 20.0.1." *Report*.

Bialowas, G., Diambra, A., and Nash, D. (2016). "Small strain stiffness evolution of reconstituted medium density chalk." *1st IMEKO TC-4 International Workshop on Metrology for Geotechnics*.

Bolton, M. and Whittle, R. (1999). “A non-linear elastic/perfectly plastic analysis for plane strain undrained expansion tests.” *Géotechnique*, 49(1), 133–141.

Buckley, R., Jardine, R., and Kontoe, S. (2021). “In situ testing in low-medium density structured chalk.” *International Conference on Site Characterisation ISC6*.

Buckley, R., Jardine, R., Kontoe, S., Parker, D., and Schroeder, F. C. (2018). “Ageing and cyclic behaviour of axially loaded piles driven in chalk.” *Géotechnique*, 68(2), 146–161.

Byrne, Y. and Whittle, R. W. (2023). “Converting between power law and hyperbolic representations of stiffness decay with strain.” *Geo-Saskatoon: Bridging Infrastucture and Resources*.

Cambridge-insitu (2023). “St nicholas at wade, source ground investigation - results of pressuremeter tests carried out by cambridge insitu ltd.” *Report*.

Campanella, R. and Stewart, W. (1991). “Downhole seismic cone analysis using digital signal processing.

Cao, L. F., Teh, C. I., and Chang, M. (2002). “Analysis of undrained cavity expansion in elasto-plastic soils with non-linear elasticity.” *International Journal for Numerical and Analytical Methods in Geomechanics*, 26(1), 25–52.

Ciavaglia, F., Carey, J., and Diambra, A. (2017). “Monotonic and cyclic lateral tests on driven piles in chalk.” *Proc. of the ICE Geotech. Eng.*, 170(4), 353–366.

Clayton, C. (2011). “Stiffness at small strain: research and practice.” *Géotechnique*, 61(1), 5–37.

Cox, B., Stolte, A., Stokoe II, K., and Wotherspoon, L. (2018). “A direct-push crosshole test method for the in-situ evaluation of high-resolution p-and s-wave velocity.” *Geotechnical Testing Journal*, 42.

Entezari, I., Sharp, J., and Mayne, P. (2022). *A data-driven approach to predict shear wave velocity from CPTu measurements*. CRC Press Boca Raton, 374–380.

Garofalo, F., Foti, S., Hollender, F., Bard, P., Cornou, C., Cox, B. R., Dechamp, A., Ohrnberger, M., Perron, V., and Sicilia, D. (2016). “Interpacific project: Comparison of invasive and non-invasive methods for seismic site characterization. part ii: Inter-comparison between surface-wave and borehole methods.” *Soil Dynamics and Earthquake Engineering*, 82, 241–254.

Gibbs, P., Pedersen, R., Krogh, L., Christopher, N., Sampurno, B., and Nielsen, S. (2018). “Challenges in marine seismic cone penetration testing.” *Cone Penetration Testing 2018: Proceedings of the 4th International Symposium on Cone Penetration Testing (CPT’18), 21-22 June, 2018, Delft, The Netherlands*, CRC Press, 303.

Hen-Jones, R., Comber, G., Worthington, P., Garantini, S., and Buckley, R. (2024). “Towards the development of a standard for the ps suspension logger.” *7th International Conference on Geotechnical and Geophysical Site Characterization (ISC)*.

Jardine, R., Buckley, R., Liu, T., Byrne, B., Kontoe, S., J., McAdam, R. A., Schranz, F., and Vinck, K. (2023). “The axial behaviour of piles driven in chalk - géotechnique - online ahead of print doi: 10.1680/jgeot.22.00041.

Karl, L., Haegeman, W., and Degrande, G. (2006). “Determination of the material damping ratio and the shear wave velocity with the seismic cone penetration test.” *Soil Dynamics and Earthquake Engineering*, 26(12), 1111–1126.

Lawrence, J. (2024). “Personal communication".

Liao, T. and Mayne, P. (2006). “Automated post-processing of shear wave signals.” *Proceedings of the 8th US National Conference on Earthquake Engineering, San Francisco. pp*, 460.1–460.10.

Liu, T., Ferreira, P., Vinck, K., Coop, M., Jardine, R., and Kontoe, S. (2022). “The behaviour of a low-to-medium density chalk under a wide range of pressure conditions.” *Soils and Foundations*.

Lord, J. A., Clayton, C. R. l., and Mortimore, R. N. (2002). “Engineering in chalk.” *Report*, CIRIA.

Lunne, T. (2010). “The cpt in offshore soil investigations–a historic perspective. jk mitchell lecture.” *Proceedings of the 2nd International Symposium on the Cone Penetration Test, CPT*, Vol. 10.

Masters, T. A., Juszkiewicz, P., Mandolini, A., and Christian, H. (2019). “A critical appraisal of the benefits of and obstacles to gaining quality data with offshore seismic cpt and ps logging.” *Offshore Technology Conference*, Offshore Technology Conference.

Matthews, M. C., Clayton, C. R. I., and Own, Y. (2000). “The use of field geophysical techniques to determine geotechnical stiffness parameters.” *Proceedings of the ICE Geotech Eng*, 143(1), 31–42.

Mayne, P. (2020). "Use of in-situ geotechnical tests for foundation systems." *Proceedings of the Széchy Károly Emlékkonferencia*, Hungarian Geotechnical Society, Budapest.

McAdam, R., Buckley, R., Schranz, F., Byrne, B., Jardine, R., and Kontoe, S. (2024). "Monotonic and cyclic lateral loading of piles in low to medium density chalk - under review.

Mortimore, R. (2014). *Logging the Chalk*. Whittles publishing, Scotland.

Mortimore, R. N. (2022). "Chalk: all we need is a fracture log!." *Quarterly Journal of Engineering Geology and Hydrogeology*, 55(1), 1–31.

Parasie, N., Franken, T., and Peuchen, J. (2022). *Assessment of seismic cone penetration testing for small strain shear modulus*. CRC Press, 203–208.

Pedone, G., Kontoe, S., Zdravković, L., Jardine, R., Vinck, K., and Liu, T. (2023). "Numerical modelling of laterally loaded piles driven in low-to-medium density fractured chalk." *Computers and Geotechnics*, 156, 105252.

Prabhu, K. M. (2014). *Window functions and their applications in signal processing*. Taylor and Francis.

Rice, A. H. (1984). "The seismic cone penetrometer." *Phd thesis*.

Rieman, L., Buckley, R., Shinde, N., and Wheeler, S. (2024). "A modified linear-elastic model for calibration of resonant column devices accommodating drive system compliance." *Géotechnique - in press*.

Stokoe, K. (2008). "The increasing role of seismic measurements in geotechnical engineering." *The Sixteenth Buchanan Lecture*, University of Texas at Austin.

Stolte, A. C. and Cox, B. R. (2019). "Towards consideration of epistemic uncertainty in shear wave velocity measurements obtained via scpt." *Canadian Geotechnical Journal*, 57(1), 48–60.

Stuyts, B., Jurado, C. S., Bautista, D. G., and Kheffache, A. (2022). *Bayesian estimation of small-strain shear modulus from offshore CPT tests in the North Sea*. CRC Press, 722–727.

Taborda, D. M., Zdravković, L., Potts, D. M., Burd, H. J., Byrne, B. W., Gavin, K. G., Houlsby, G. T., Jardine, R. J., Liu, T., and Martin, C. M. (2019). "Finite-element modelling of laterally loaded piles in a dense marine sand at dunkirk." *Géotechnique*, 70(11), 1014–1029.

Vinck, K. . (2021). “Advanced geotechnical characterisation to support driven pile design at chalk sites.” *Phd thesis*.

Vinck, K., Liu, T., Jardine, R., Kontoe, S., Ahmadi-Naghadeh, R., Buckley, R., Byrne, B., Lawrence, J., Mcadam, R., and Schranz, F. (2022). “Advanced in-situ and laboratory characterisation of the alpaca chalk research site, géotechnique, online ahead of print.

Wen, K., Kontoe, S., Jardine, R. J., and Liu, T. (2023). “An axial load transfer model for piles driven in chalk.” *Journal of Geotechnical and Geoenvironmental Engineering*, 149(11), 04023107.

Whittle, R. W., Palix, E., and Donaghy, D. (2017). “The influence of insertion process on determining the stiffness characteristics of chalk, using pre-bored, self-bored and pushed pressuremeters.

Winn, R., Anderson, T., and Carter, L. (1962). “A preliminary study of factors influencing cement bond logs.” *Journal of Petroleum Technology*, 14(04), 369–372.

NOTATION

The following symbols and abbreviations are used in this paper:

d_1, d_2 = vertical distance from ground level to receiver 1 and 2

d_s = source offset

f_c = cut off frequency for filtering

f_s = CPT sleeve friction

G_0 = small stain shear modulus ;

$G_{0,lab}$ = small strain shear modulus measured in the laboratory

$G_{0,insitu}$ = small strain shear modulus measured in situ

$G_{s,hh}$ = secant shear modulus in PMT (Eq. 8)

G_y = shear modulus at first yield of the material in PMT

Lin_1, Lin_2 = Linearity estimates at successive depths

q_t = corrected CPT cone resistnace

q_u = unconfined compressive strength

S(f) = frequency spectrum of the filtered data

u_1 = pore pressure measured at the tip position

u_2 = pore pressure measured at the shoulder position

V_s = shear wave velocity

V_p = compression wave velocity

= horizontally propagating vertically travelling shear wave velocity or small-strain shear mo

$V_{s,hh}$ or G_{hh} = horizontally propagating horizontally travelling shear wave velocity or small-strain shear r

$V_{x,y}$ = Covariance matrix of X_k and Y_k

X_k = signal sampled at d_1 and sample time k

Y_k = signal sampled at d_2 and sample time k

α, β = Parameters in the expression for secant shear modulus $G_{s,hh}$

γ_{el} = yield strain in PMT

ΔL = travel distance (L_1- L_2)

Δt = elapsed travel time

λ = wavelength = Velocity/frequency

ρ = soil density

σ = standard deviation

ϕ_{xy} = cross-correlation function

BE = bender element test

CBL = cement bond length test

CC = cross-correlation method to calculate Δt

CCC = cross-correlation coefficiant

CH = Crosshole seismic

CPT = cone penetration test

DH = Downhole seismic

FI = Fracture index

HPD = high pressure dilatometer

Lin = linearity

LL = liquid limit

mAOD = metres above ordnance datum

PSL = PS logging

PMT = pressuremeter test

PWP = pore water pressure

P-P = Peak-to-peak method to calculate Δt

RC = resonant column

RL = reduced level

RP = reverse polarity method to calculate Δt

RPM = reamining pressuremeter

SB = shear beam

SBP = self-boring pressuremeter

SSP = signal shape parameter

STC = seismic trace characterisation

WC = water content

List of Tables

Loc	Type	RL (mAOD)	Min RL (mAOD)	Tip Deviation (°)	Comment
BH1	Borehole	6.7	-18.3	0.4	CBL, Deviation survey
BH2	Borehole	6.7	-18.3	0.1	CBL, Deviation survey, PMT
BH3	Borehole	6.7	-18.3	0.5	CBL, Deviation survey
BH4	Borehole	6.8	-37.2	0.1	CBL, Density, Deviation survey, PMT
CPT1	CPT	6.7	1.6	-	Refusal at 5.1mbgl
CPT2	CPT	6.7	2.2	-	Refusal at 4.5mbgl
CPT3	CPT	6.7	-9.3	-	Refusal at 16mbgl
CPT4	CPT	6.7	2.1	-	Refusal at 4.6mbgl
CPT5	CPT	6.7	2.1	-	Refusal at 4.6mbgl

TABLE 1. Invasive investigation - boreholes and cone penetration tests

Loc	Type	Mean start RL (mAOD)	Max depth RL (mAOD)	Interval (m)	Receiver spacing (m)	Source offset (m)	Logging frequency (kHz)
BH1	DH	4.1	-17.1	1	2	2.15	16
BH2	DH	4.1	-17.1	1	2	2.15	16
BH3	DH	4.1	-17.1	1	2	2.15	16
BH4	DH	4.1	-35.8	1	2	2.15	16
BH4 to 1	CH	4.1	-35.8	1	-	-	16
BH1	PSL	0.7	-13.4	0.5	1	2.125	200
BH2	PSL	0.7	-13	0.5	1	2.125	200
BH3	PSL	0.7	-13	0.5	1	2.125	200
BH4	PSL	0.8	-33.2	0.5	1	2.125	200
SCPT1	SCPT	6.5	4.5	0.25	0.5	2	5
SCPT2	SCPT	6.2	4.2	0.5	0.5	2	5
SCPT3	SCPT	6.2	4.2	0.5	0.5	2	5
SCPT4	SCPT	1.3	-2.2	0.5	0.5	2	5
SCPT5	SCPT	6.5	3.25	0.25	0.5	2	5
SCPT6	SCPT	6.5	1.25	0.25	0.5	2	5

TABLE 2. Testing programme - geophysics

Location	No.	Type	RL (mAOD)	Probe	Max pressure (kPa)	Comment
BH2	1	Self-bored	2.8	SBP	4259	-
BH2	2	Self-bored	0.7	SBP	3789	-
BH2	3	Self-bored	-4.8	SBP	-	Refusal on flints
BH2	4	Pre-bored	-5.5	HPD	3555	-
BH2	5	Self-bored	-9.8	SBP	-	Refusal on flints
BH2	6	Pre-bored	-11.2	RPM	3897	-
BH4	1	Pre-bored	-5.3	RPM	707	-
BH4	2	Pre-bored	-11.5	HPD	3405	Terminated early - leak
BH4	3	Pre-bored	-12.7	RPM	-	Failed to form a pocket

TABLE 3. Testing programme - pressuremeter testing

Method	**DH**	**CH**	**PSL**	**SCPT**
Total No.	683	127	292	55
Cross-correlation	89%	14%	80%	27%
Cross-correlation - 2nd peak	3%		5%	
Cross-correlation with window	-	24%	1%	51%
Reverse polarity - before peak	4%	54%	4%	-
Reverse polarity - after peak	-	6%	-	-
Peak to Peak	4%	2%	10%	22%

TABLE 4. Interpretation methods

Location	No.	RL (mAOD)	α (MPa)	β	G_y (MPa)	G_{hh} (MPa)	γ_{el} (%)
BH2	1	2.8	43.2	0.723	252	1003	1.2e-3
BH2	2	0.7	46.7	0.771	207	755	5.2e4
BH2	4	-5.5	95.1	0.796	409	1435	1.7e4
BH2	6	-11.2	31.9	0.797	108	378	5.1e4
BH4	1	-5.3	88.3	0.733	541	2115	6.8e4

TABLE 5. Pressuremeter results

List of Figures

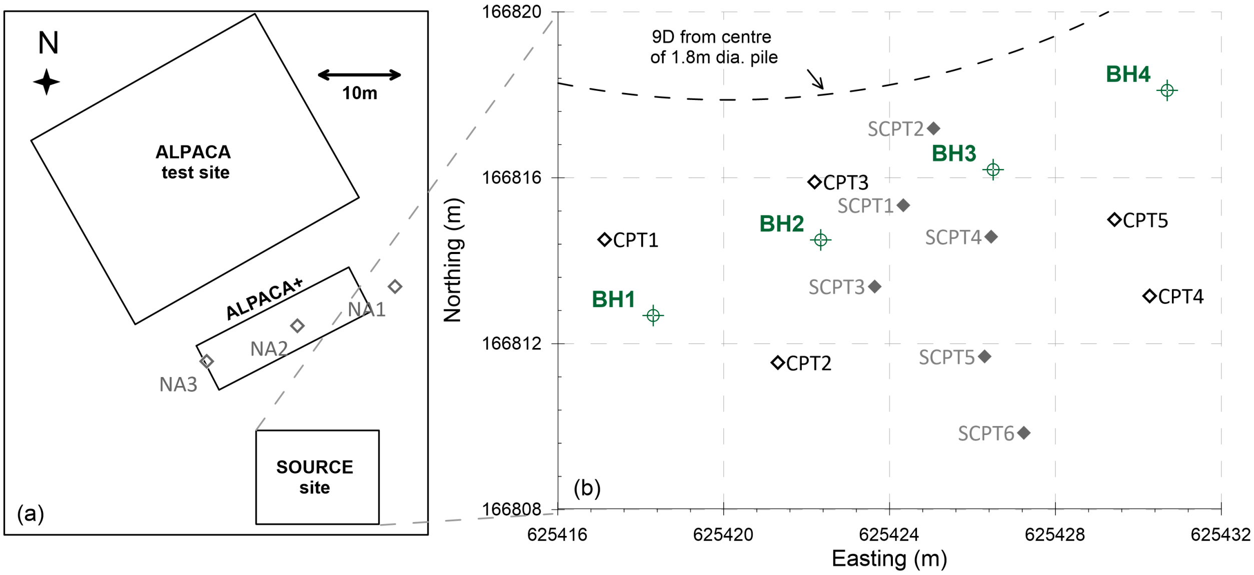

Fig. 1. Location plan (a) SOURCE site in relation to previous pile testing (b) Layout of boreholes, cone penetration tests and seismic cone penetration tests

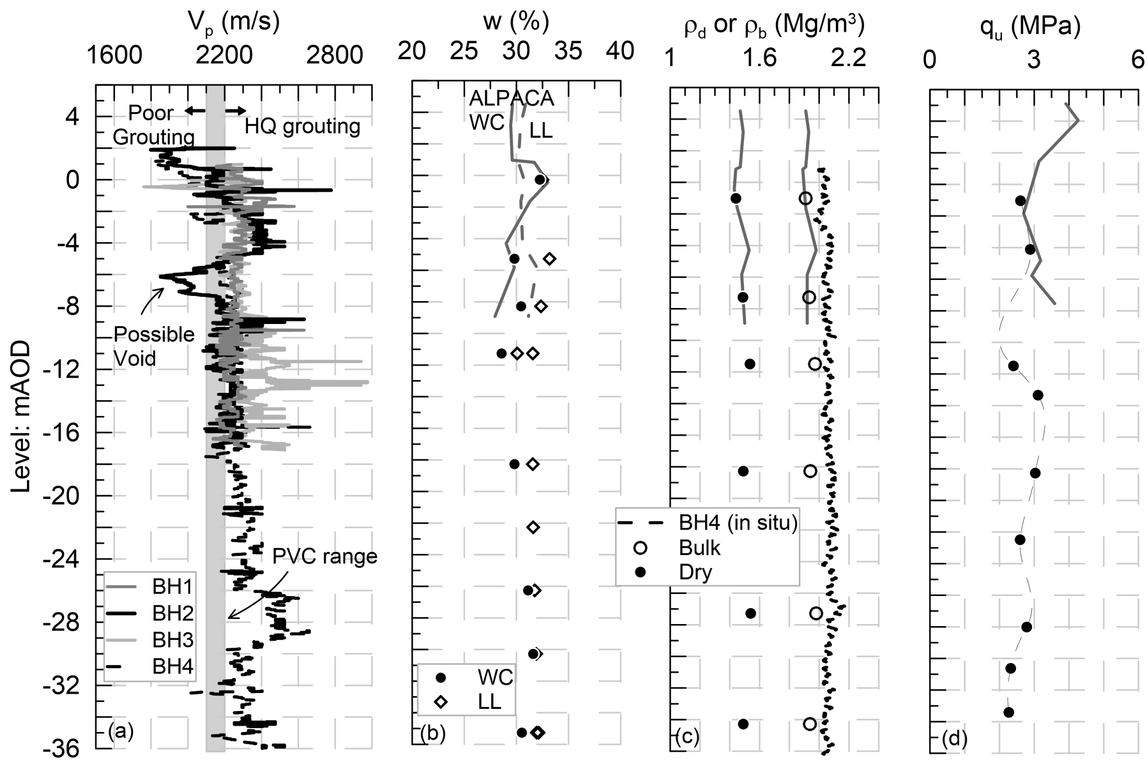

Fig. 2. (a) Cement Bond Length testing (b) natural water content (WC) and liquid limits (LL) (c) in situ and laboratory densities (d) unconfined compressive strengths, q_u

(a)

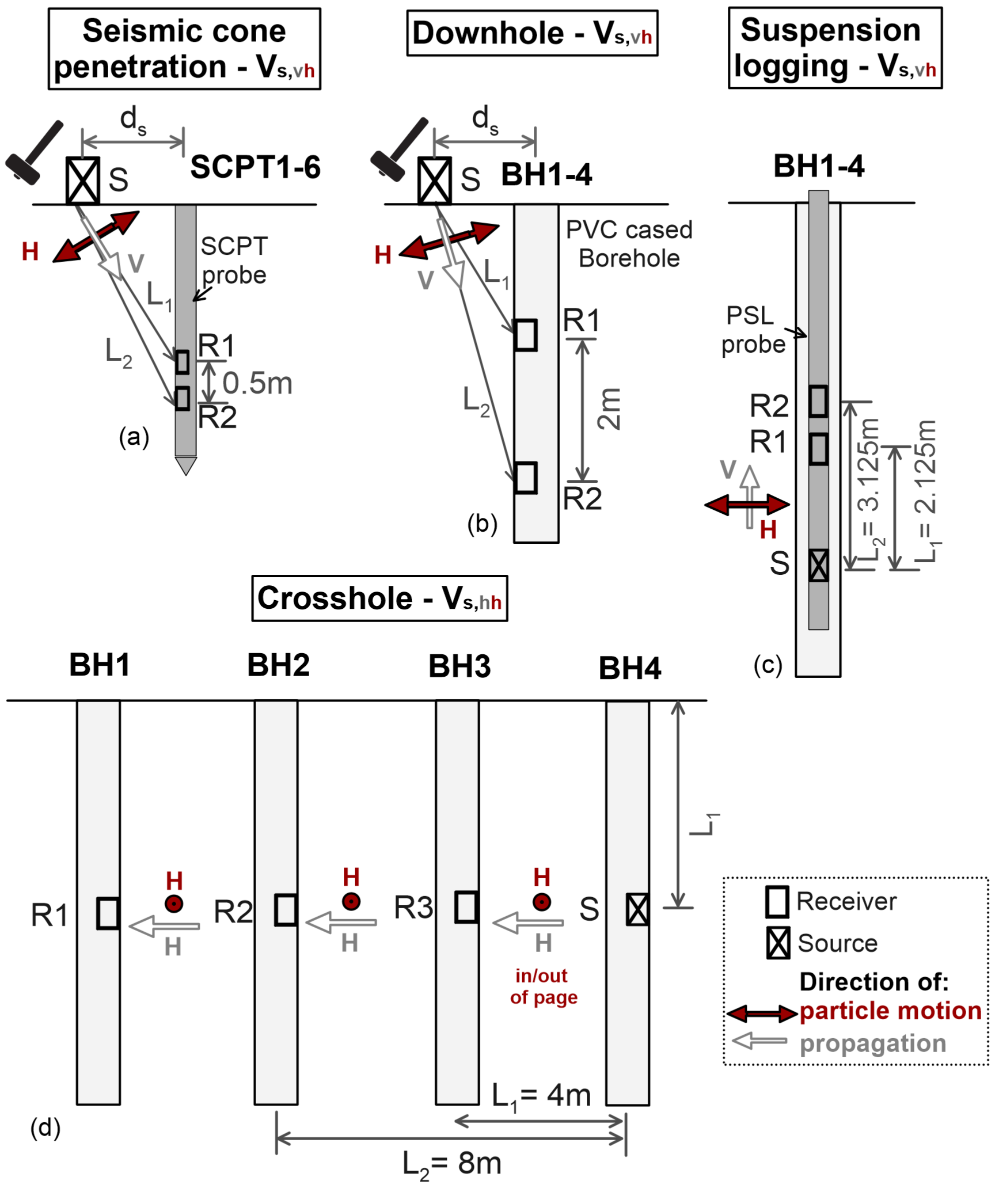

Fig. 3. Schematic of geophysical test methods considered (a) downhole borehole geophysics (b) seismic cone penetration test (c) P-S logging (d) crosshole borehole geophysics

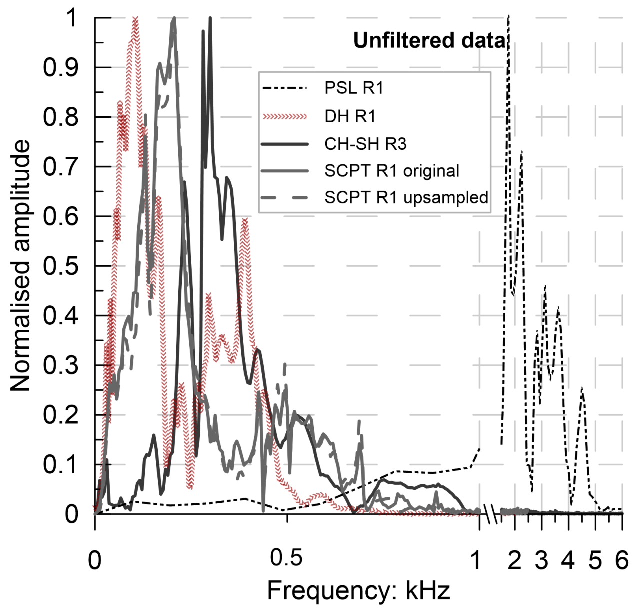

Fig. 4. Frequency spectra of typical signals recorded in each test type

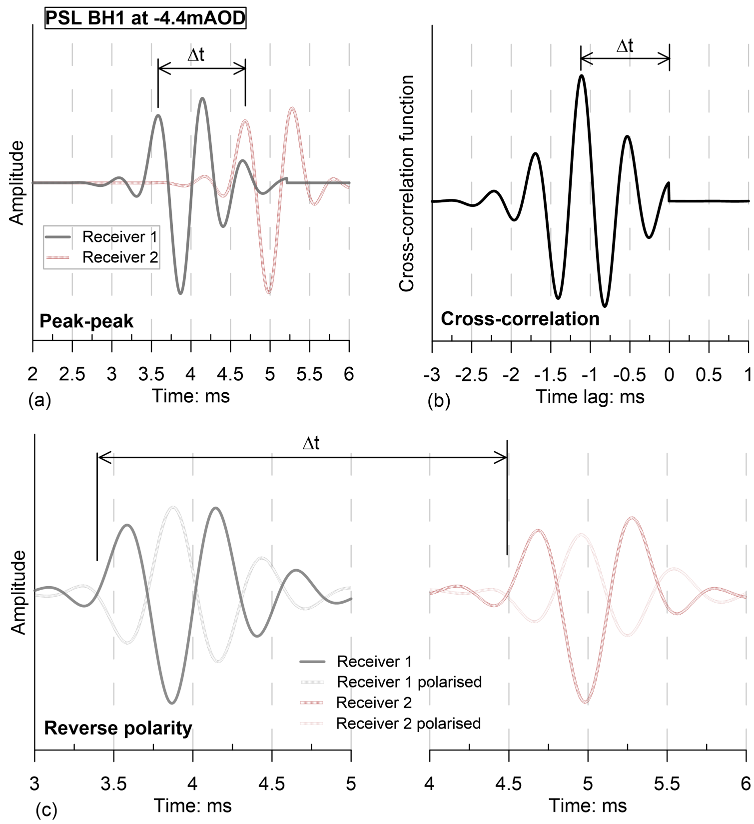

Fig. 5. Example interpretation of travel times from windowed dual receiver PSL data (a) peak to peak (b) cross-correlation (c) reverse polarity

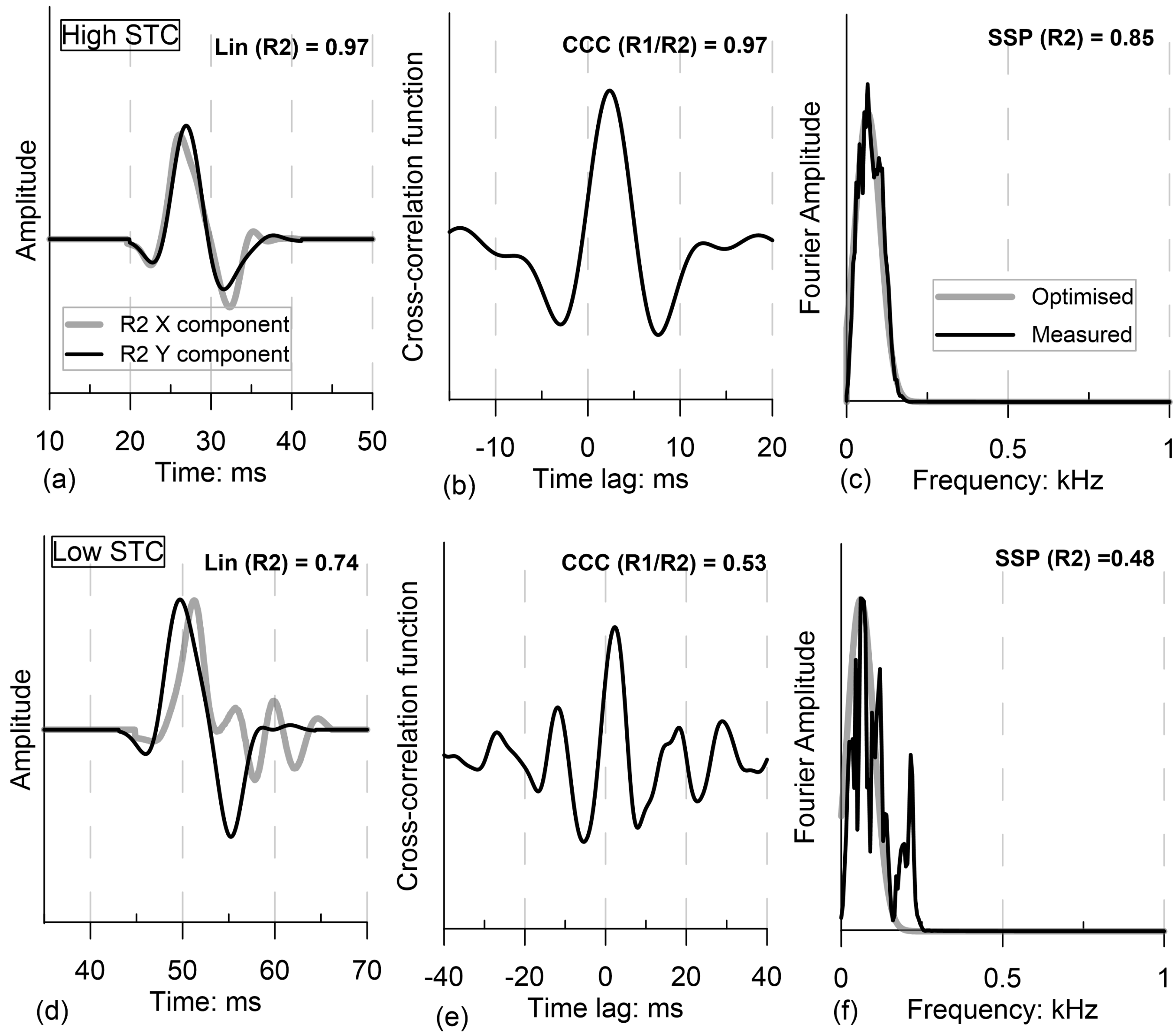

Fig. 6. Example of signal trace characteristic (Baziw and Verbeek, 2017), high, STC=1.03 (a) linearity estimation (b) cross-correlation function and coefficient (c) signal shape parameter; low, STC=0.63 (d) linearity estimation for R2 (e) cross-correlation function (R1/R2) and coefficient (f) signal shape parameter (R2)

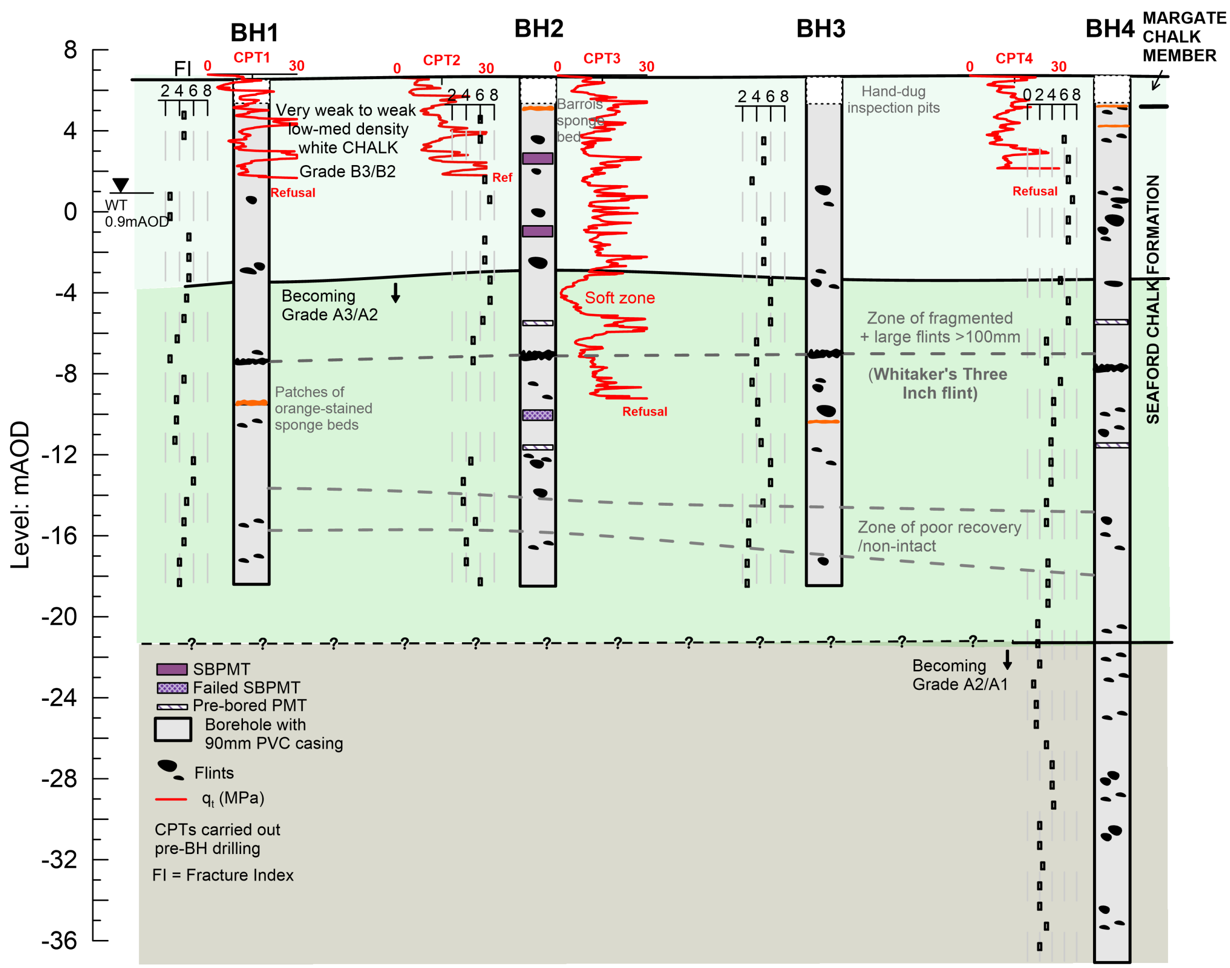

Fig. 7. Cross-section across the study area highlighting main features identified in detailed core logging

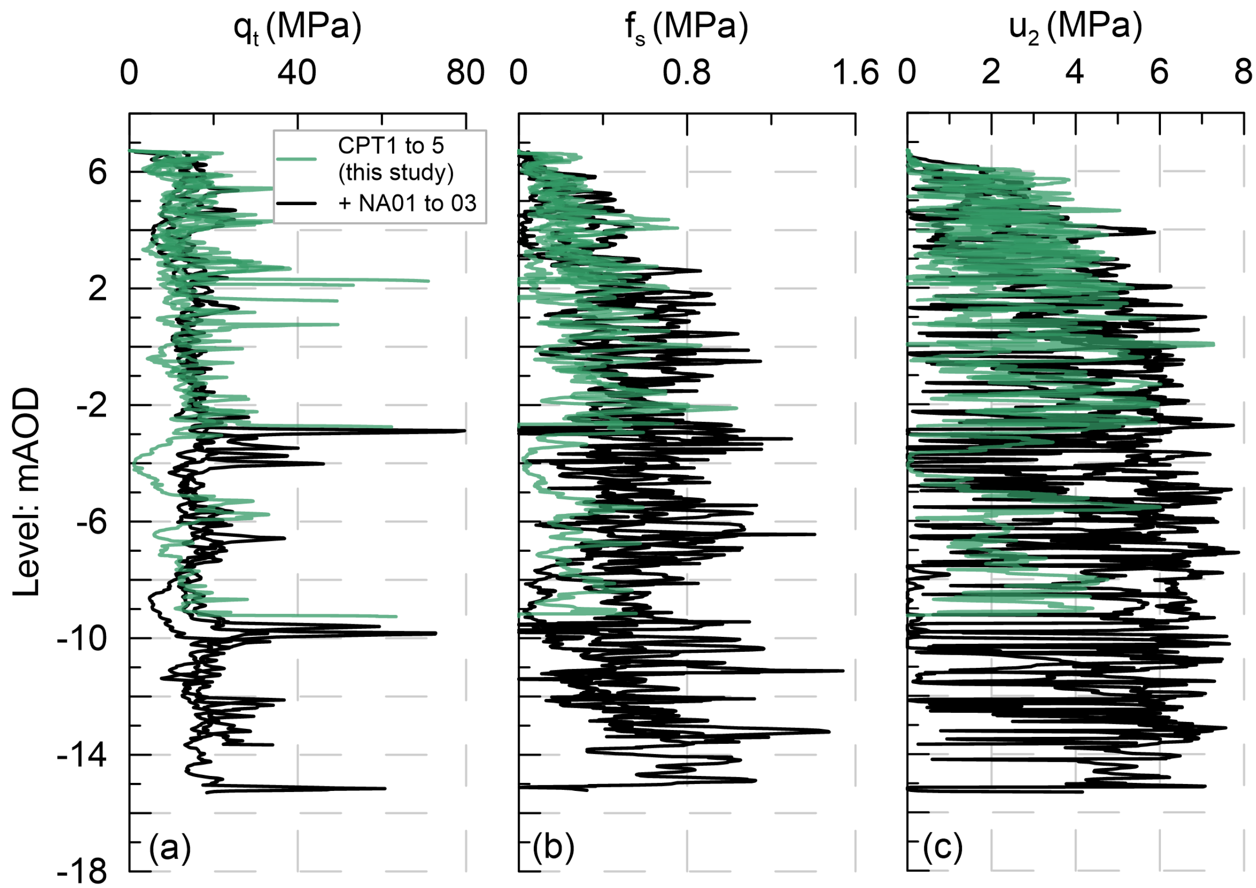

Fig. 8. Cone penetration tests at the SOURCE site (CPT1 to CPT5) compared to results at the nearby ALPACA+ test site

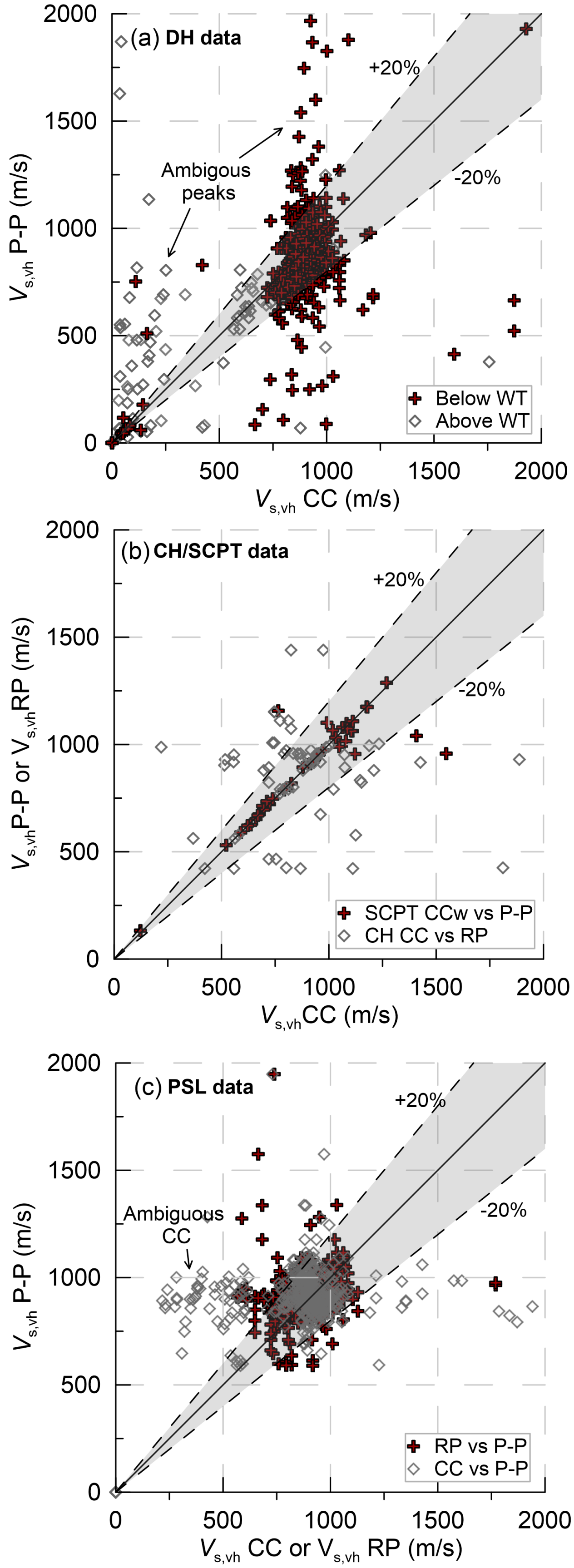

Fig. 9. Comparison of V_s measurements calculated using different methods to calculate elapsed time (a) DH (b) CH/SCPT (c) PSL

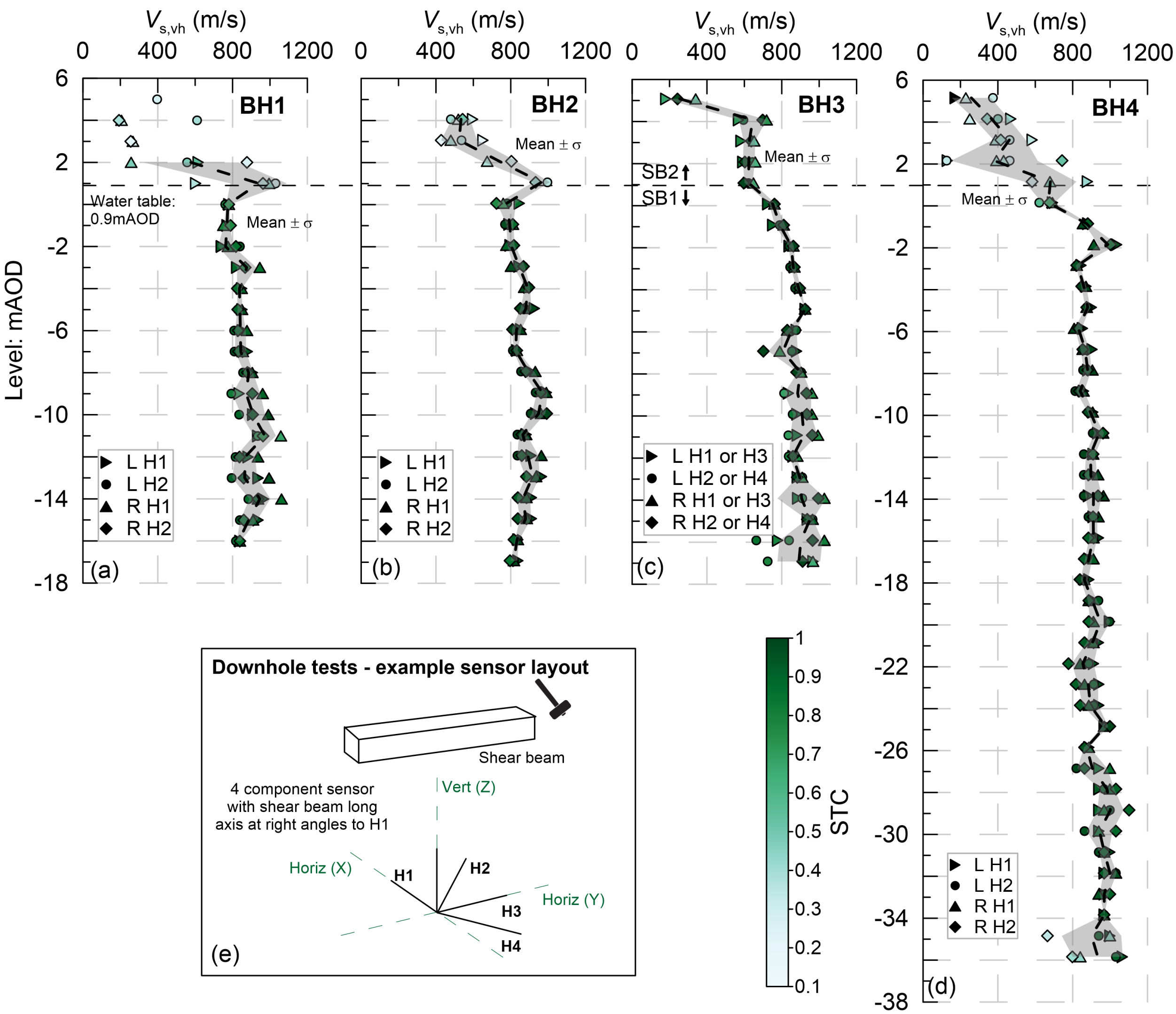

Fig. 10. Shear wave velocities ($V_{s,vh}$) interpreted from downhole testing (a) BH1 (SB1) (b) BH2 (SB1) (c) BH3 (SB1/2) (d) BH4 (SB1) (e) sensor orientation

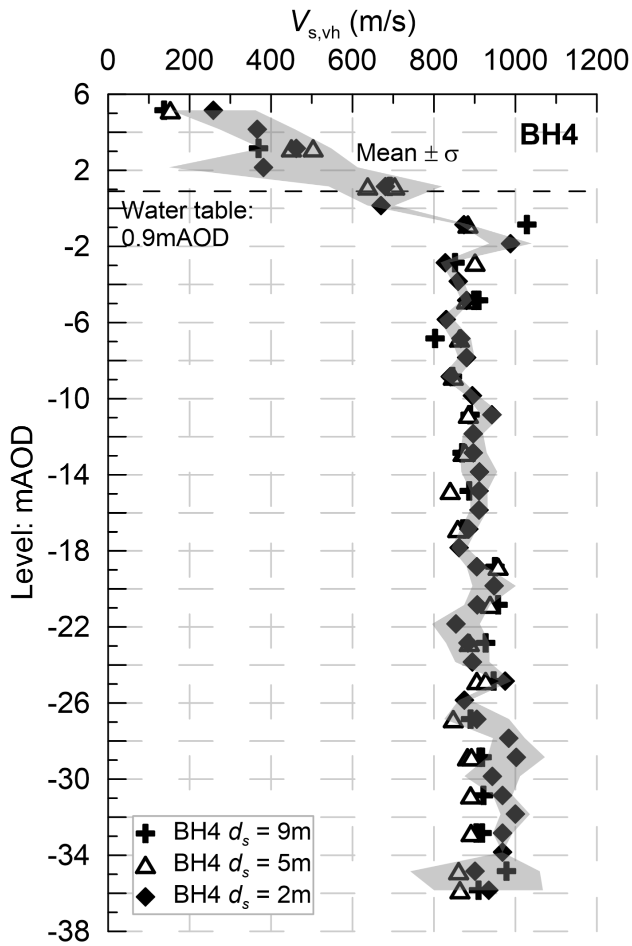

Fig. 11. Influence of source offset, d_s, on shear wave velocities ($V_{s,vh}$) interpreted from downhole testing

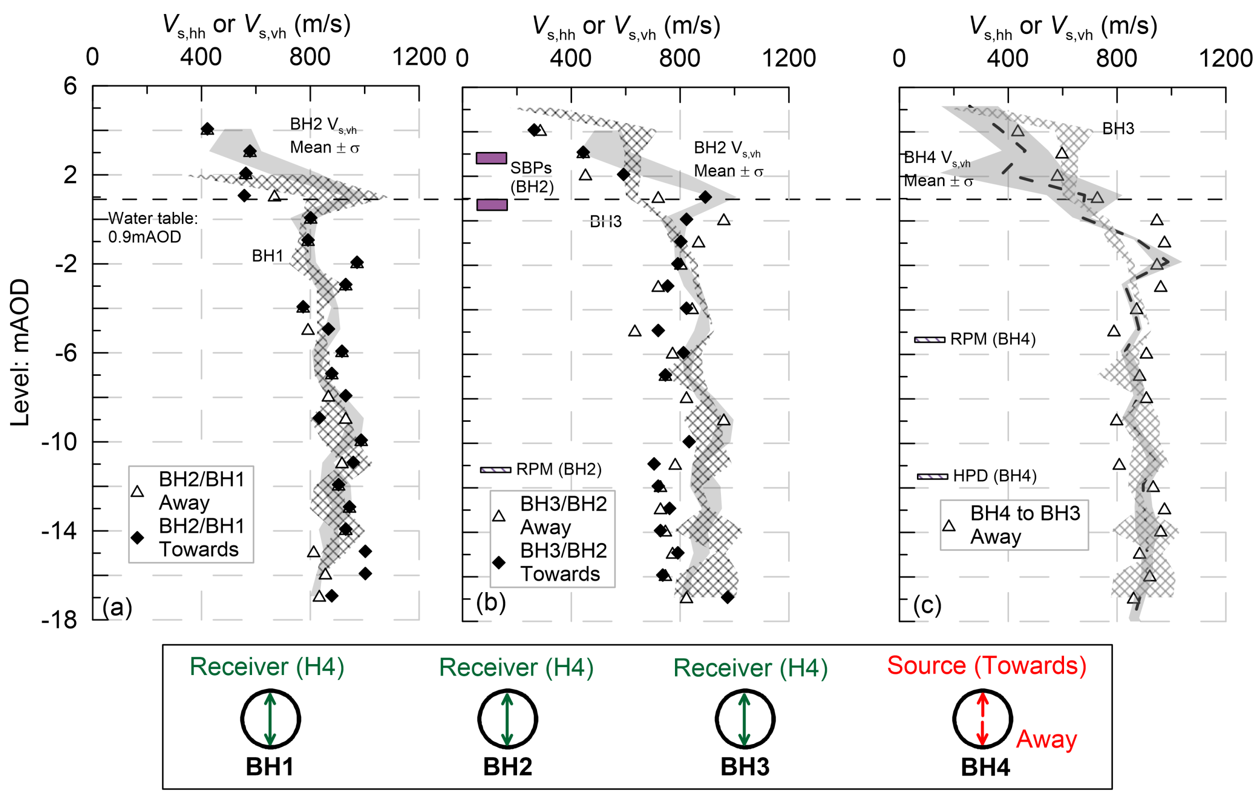

Fig. 12. Shear wave velocities ($V_{s,hh}$) interpreted from crosshole testing (a) BH2/BH1 (b) BH3/BH2 (c) BH4 (Receiver)/BH3

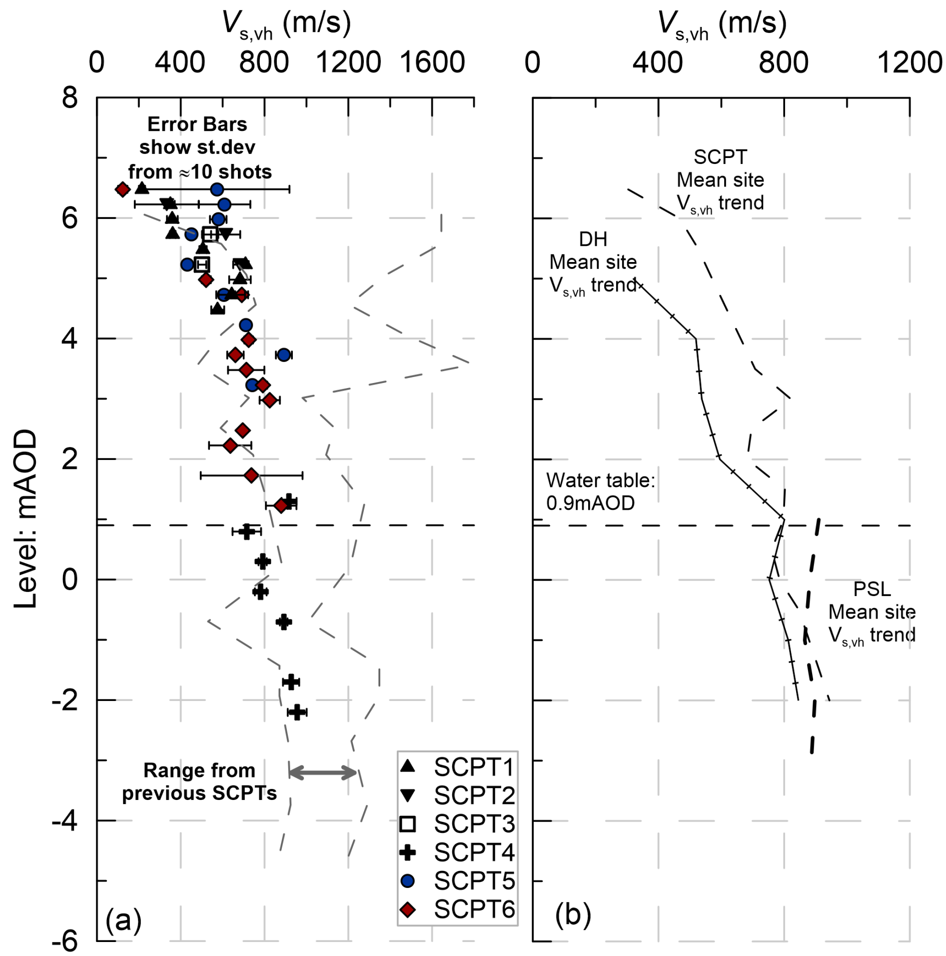

Fig. 13. (a) seismic cone penetration test results from across the site (b) trend in SCPT ($V_{s,vh}$) compared with downhole and PSL logging ($V_{s,vh}$) trends

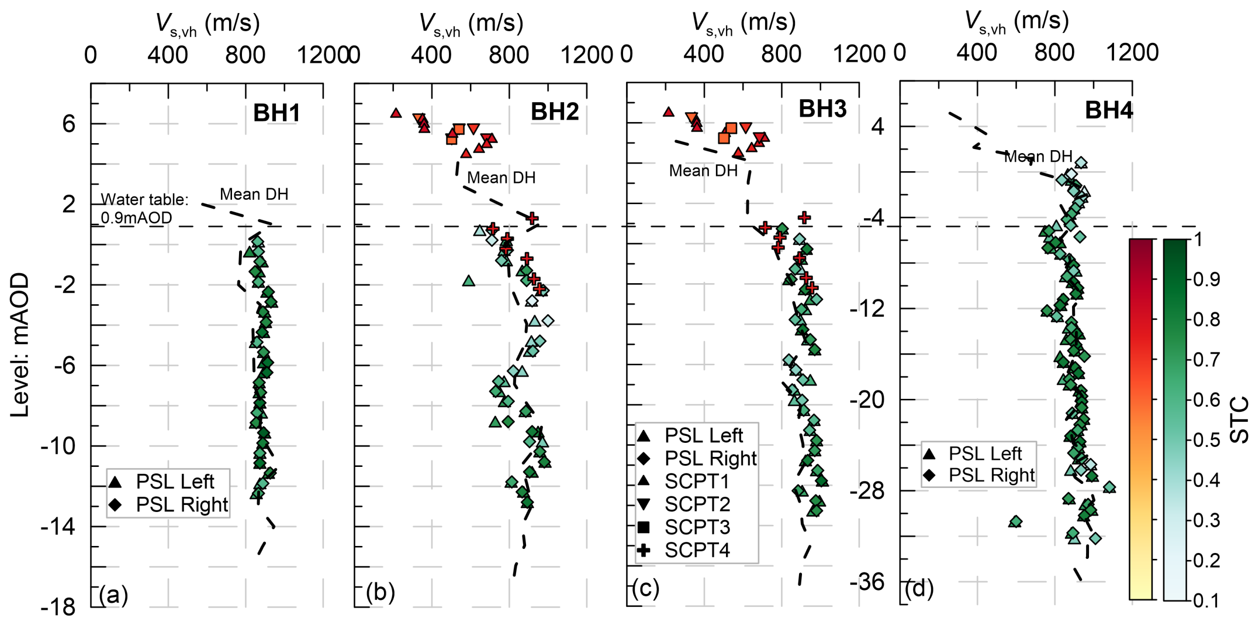

Fig. 14. Shear wave velocities ($V_{s,vh}$) interpreted from PS logging (a) BH1 (b) BH2 (c) BH3 (d) BH4. Nearby SCPTs are also plotted

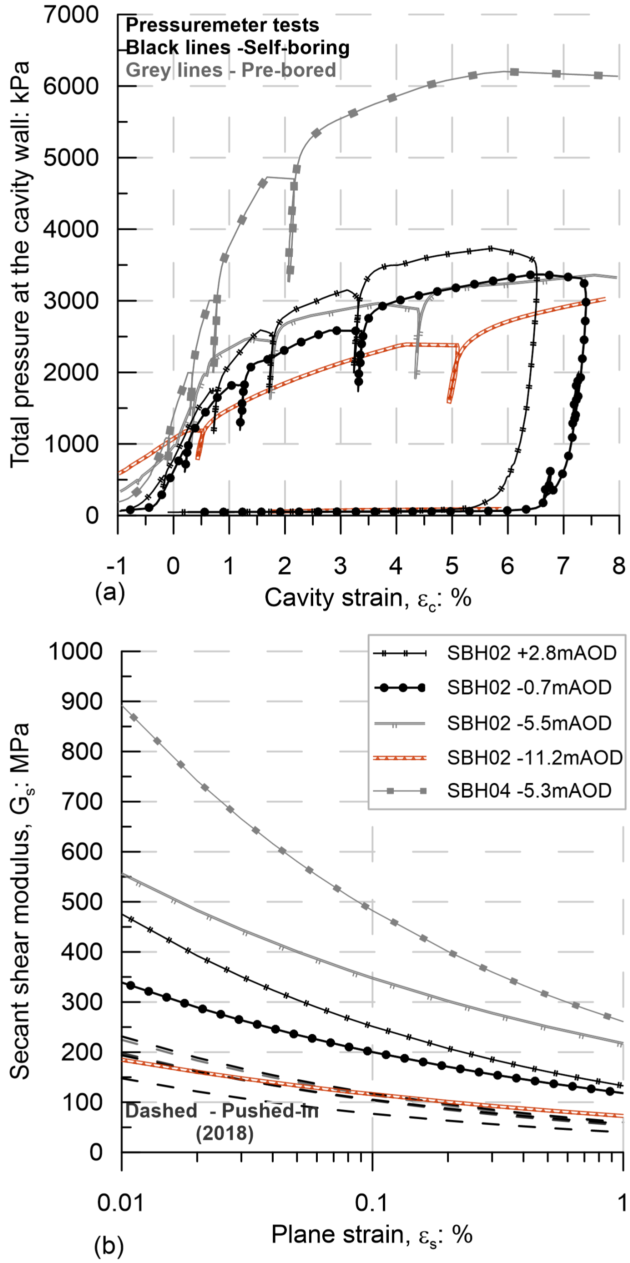

Fig. 15. Pressuremeter tests (a) total pressure versus cavity strain (b) Secant shear modulus versus plane strain

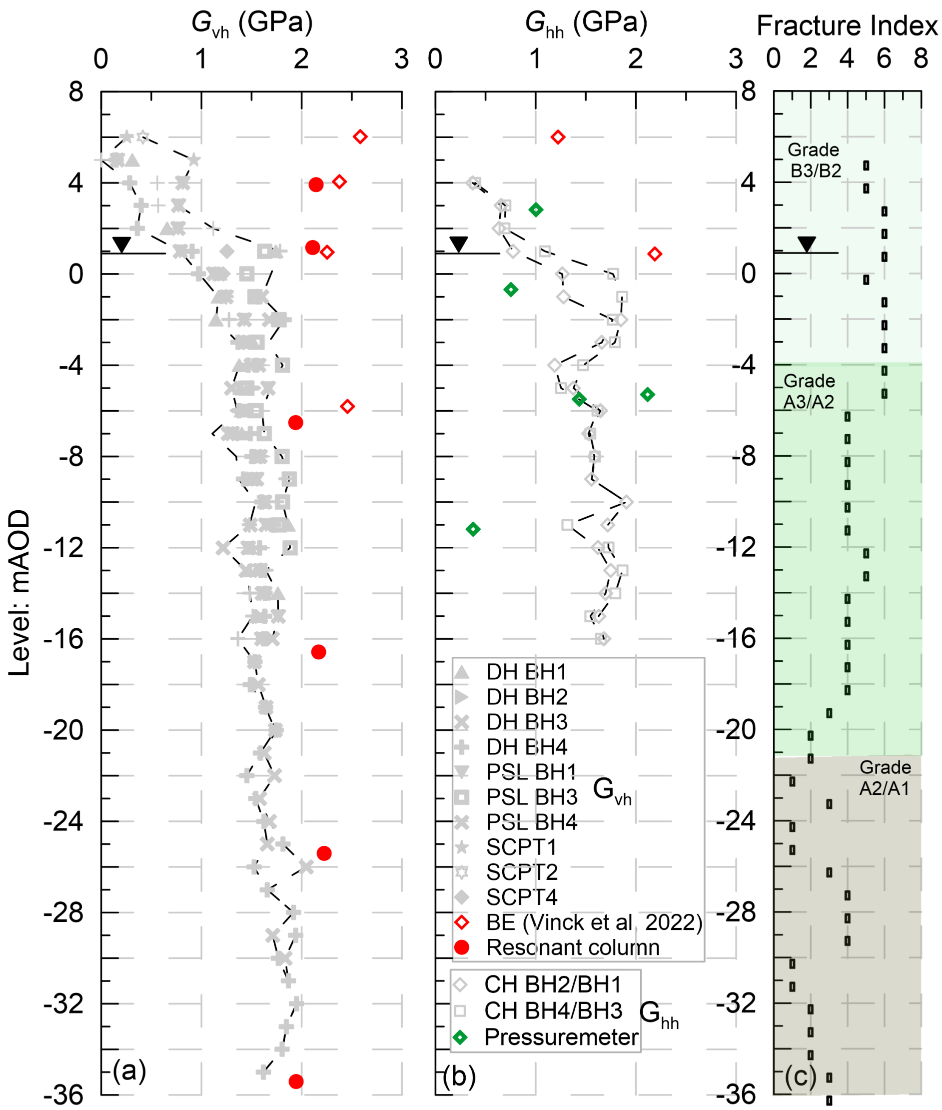

Fig. 16. Average trends in (G_{vh}) and (G_{hh}) from multiple methods (a) G_{vh} from DH, PSL, and SCPT (b) G_{hh} from crosshole and PMT (c) average fracture index from all 4 boreholes